

Trotter Error and Orbital Transformations in Quantum Phase Estimation

Marvin Kronenberger¹, Mihael Erakovic¹, and Markus Reiher^{1,*}

¹ETH Zürich, Department of Chemistry and Applied Biosciences,
Vladimir-Prelog-Weg 2, 8093 Zürich, Switzerland

*Corresponding author: mreiher@ethz.ch

February 20, 2026

Abstract

Quantum computation with Trotter product formulae is straightforward and requires little overhead in terms of logical qubits. The choice of the orbital basis significantly affects circuit depth, with localised orbitals yielding lowest circuit depths. However, literature results point to large Trotter errors incurred by localised orbitals. Here, we therefore investigate the effect of orbital transformations on Trotter error. We consider three strategies to reduce Trotter error by orbital transformation: (i) The a priori selection of an orbital basis that produces low Trotter error. (ii) The derivation of an orbital basis that produces a ground state energy free of Trotter error (as we observed that the Trotter error is a continuous function in the Givens-rotation parameter, from which continuity of this error upon orbital transformation can be deduced). (iii) Application of propagators that change the computational basis between Trotter steps. Our numerical results show that reliably reducing Trotter error by orbital transformations is challenging. General recipes to produce low Trotter errors cannot be easily derived, despite analytical expressions which suggest ways to decrease Trotter error. Importantly, we found that localised orbital bases do not produce large Trotter errors in molecular calculations, which is an important result for efficient QPE set-ups.

Keywords

quantum computing; quantum chemistry; Trotter error; orbital basis; randomised product formula

1. Introduction

Accurate quantum chemical calculations of highly correlated electronic structures in chemistry require high-accuracy multi-configurational methods [1–4]. The exponential scaling of the Hilbert space dimension with the size of the active orbital space remains a key hurdle for the development of such methods on classical hardware. Quantum computers have an exponential advantage in the number of quantum versus classical bits required to encode elements of this Hilbert space [5]. This motivates the development of algorithms on quantum hardware which allow for tackling strongly correlated molecules.

Quantum phase estimation (QPE) [6] estimates the eigenenergies of arbitrary Hamiltonians on fault-tolerant quantum hardware [7] and requires the implementation of a unitary propagator U , whose eigenphases ω_k deliver the eigenenergies E_k of the Hamiltonian \hat{H} [7, 8]. The probability with which a binary representation of each eigenphase ω_k can be measured is $|\langle\psi(0)|\psi_k\rangle|^2$ [9]. Here, $|\psi(0)\rangle$ denotes the input state which will be evolved in time via Hamiltonian simulation and $|\psi_k\rangle$ is the eigenstate of \hat{H} corresponding to the eigenenergy E_k .

To compute the ground state energy E_0 to some accuracy ϵ , two quantities determine the total quantum-resource cost of the QPE circuit. First, the number of qubits and quantum gates required to prepare an initial state $|\psi(0)\rangle$, which has sufficiently high overlap with the target ground state wave function $|\psi_0\rangle$ (state-preparation cost). Second, the number of qubits and quantum gates required to implement the unitary propagator U (Hamiltonian-simulation cost).

Within QPE, Hamiltonian simulation for time t_{total} determines the ground state energy E_0 to a desired accuracy ϵ (where $t_{\text{total}} \propto 1/\epsilon$) by implementation of the unitary operation $U = \exp(-i\hat{H}t_{\text{total}})$ on a quantum device. A plethora of choices for the numerical representation of the Hamiltonian \hat{H} exists [10–21]. This choice directly affects both the cost of state preparation [22–26] and the Hamiltonian simulation itself [12–15, 18–21]. Here, we consider the second-quantised electronic Hamiltonian expressed in a spin orbital basis, which is commonly employed in the literature [8, 9, 11, 15, 27].

Various schemes are available to implement the time-evolution operator U on a quantum computer. A Trotter product formula can be employed to split the exponential of the operator sum into products of single operator exponentials [7, 8, 28, 29]

$$U = \exp(-i\hat{H}t_{\text{total}}) = \exp\left(\sum_k^{\Gamma} -i\hat{H}_k t_{\text{total}}\right) = \lim_{s \rightarrow \infty} \prod_k^{\Gamma} \left(\exp(-i\hat{H}_k t)\right)^s, \quad (1)$$

where $t = t_{\text{total}}/s$ denotes the time evolution t associated with each so-called ‘Trotter step’. The single-operator exponentials $\exp(-i\hat{H}_k t)$ can then be translated into quantum circuits as described, for example, in Refs. [9, 30]. In practice, the number of Trotter steps s (‘Trotter step number’) in Eq. (1) should be chosen such that the error $|\Delta E_0|$ of the ground state energy E_0 is smaller than the target accuracy. For electronic structure calculations, this is typically chemical accuracy, which is characterised by Trotter errors below $0.1 - 1 \text{ mE}_h$ [11, 31].

Alongside trotterisation, several other strategies exist to propagate the wave function in the context of QPE. Implementing Linear Combinations of Unitaries (LCU) on a quantum circuit [32] allows for the representation of the time evolution operator via multi-product formulas (MPFs) [32, 33]. MPFs refer to linear combinations of trotterised propagators with different Trotter steps s . Since the sums of unitary operators are not guaranteed to construct a unitary operator, MPFs are generally non-unitary propagators and require additional ancilla qubit overhead [32]. Hamiltonian simulation is also possible with ‘qubitised’ block encodings of the Hamiltonian [34]. Evolving the wave function with the ‘walker’ operator $\mathcal{W}[\hat{H}] = \exp(-i \arccos \hat{H}/\lambda)$ [14, 25, 35, 36] instead of $U = \exp(-i\hat{H}t)$ allows error-free calculations of E_0 from QPE. The 1-norm λ denotes a normalisation constant, such that the spectrum of \hat{H}/λ is normalised. While benchmark studies [14, 15, 20, 21, 37] on proposed target molecular systems [11, 14, 23, 38–43] show lower Toffoli gate counts compared to trotterised methods, this comes at greater than approximately an order of magnitude increase in logical qubit requirements. The additional qubit requirements of qubitisation stem from the necessity to block-encode \hat{H}/λ , which requires the embedding of the Hamiltonian in a larger Hilbert space [34].

The smaller number of logical qubits required for trotterisation makes Hamiltonian simulation with trotterised product formula well suited for early future fault-tolerant hardware, which will be qubit limited. For this reason, we focus here on strategies to reduce the cost of trotterised Hamiltonian simulation. As is apparent from Eq. (1), lower Trotter step numbers s and a lower number of terms Γ in the Hamiltonian decrease the resource cost of trotterised Hamiltonian simulation. To allow for the use of larger Trotter step numbers s necessitates low Trotter errors $|\Delta E_0|$ in the ground state energy E_0 . Higher-order Trotter formulae reduce the Trotter error, but come at an exponential increase in the circuit depth of a Trotter step [44, 45]. First- and second-order Trotter formulae have therefore been predominantly employed in the literature [11, 27, 31, 46].

A variety of factors have been investigated to reduce Trotter error (independent of the order of the employed Trotter formula): Specifically, the choice of orbital basis [31], ordering of terms in the Trotter series [47] (which we denote ‘(Trotter) series-ordering’), and Hamiltonian representation [12] on Trotter error have been analysed. In recent years, several approaches for Hamiltonian simulation with product formula beyond fixed-order Trotter formula have been suggested. Ref. [48] applies tensor hypercontraction [15, 49–51] to construct the smallest possible basis, in which the electron repulsion integral tensor is diagonal. This facilitates error-free simulation of the two-body interactions in the Hamiltonian at the cost of additional qubits due to the increased basis size.

State-of-the-art simulations of electronic Hamiltonians by product formulae exploit partially randomised product formulae [37, 52, 53]. The idea to approximate Hamiltonian simulation with randomised product formulae instead of fixed-order Trotter decompositions followed from work by Childs et al. [54] and by Campbell [55]. The former authors derived tighter bounds on Trotter error for propagators with random reorderings of the terms \hat{H}_k compared to fixed series order propagators [54]. The quantum stochastic drift (qDRIFT) protocol [55] abandons Trotter series altogether and instead approximates Hamiltonian simulation by a Markovian process, where the operators $\exp(-i\hat{H}_k t)$ are randomly sampled according to the weights $|h_k|$ in \hat{H}_k of Eq. (2). These weights $|h_k|$ depend on the specific representation of the Hamiltonian terms \hat{H}_k that are employed. They generally correspond to weighted sums of the integrals h_{ij} and h_{pqrs} , as, for instance, detailed in Ref. [56]. Hamiltonian simulation with partially randomised product formula implement terms with large weights by high-order Trotter formulae. Terms with small weights are evolved by the qDRIFT protocol [37]. The cost of Hamiltonian simulation with qDRIFT scales linearly with the squared Hamiltonian 1-norm λ^2 , where $\lambda = \sum_k |h_k|$. It is well established that localised orbital bases minimise the Hamiltonian 1-norm [56] and therefore achieve the lowest-cost Hamiltonian simulation with qDRIFT.

Finding an optimal orbital basis in which to implement the large coefficient terms is, however, less straightforward. Ref. [31] is the only study which thoroughly presents numerical data of Trotter error as a function of commonly employed orbital bases. This study [31] reported comparatively large Trotter errors in local orbital bases, which is in contrast with the known correlation between upper bounds of Trotter error and sums of the absolute values of the Hamiltonian weights, i.e., the 1-norm λ [11, 37, 44]. Since the difference between canonical and localised orbitals is more pronounced for extended molecular systems [56, 57], we provide additional results on the effect of orbital localisation on Trotter error as part of this work. We investigate Trotter errors for active spaces of linear and non-linear π -conjugated molecules, π -systems in short, where the difference between canonical (i.e., delocalised) and localised orbitals is more pronounced compared to atomic, diatomic, and triatomic systems investigated in Ref. [31].

Following Childs et al. [54] and Martínez-Martínez et al. [12], we also study randomised propagators. We analyse whether randomly changing the series-ordering or

the orbital basis in each Trotter step reduces the Trotter error in the ground state energy. We emphasise that achieving error reduction by a dynamic orbital basis (compared to dynamic Trotter series-ordering) can be advantageous, since it allows for the selection of a fixed Trotter series order. To reduce circuit depth, a Trotter series order which maximises the number of gate cancellations could then be employed [58, 59]. We employ a Givens rotation representation of the orbital basis to account for a basis change. Examples where error cancellation, averaging effects, and error magnification can be observed are discussed. Finally, we discuss whether the continuity of Trotter error upon orbital transformations can be leveraged to determine an orbital basis with little or no Trotter error in the ground state energy.

2. Theory

In this section, we introduce the representations of the electronic Hamiltonian employed throughout this work. We describe how orbital transformations can be leveraged to change the basis in which the electronic Hamiltonian is expressed. We provide an overview on methods to assess Trotter error. We discuss which of these methods are suited to compare Trotter errors between different orbital bases for molecular systems and what easily obtainable quantities, which we refer to as descriptors hereafter, might correlate with Trotter error. The identification of such descriptors is desirable, since it would enable the selection of a low-Trotter-error orbital basis prior to an actual quantum computation. Finally, Section 2.5 introduces the randomised propagators studied in this work.

2.1. Representations of the electronic Hamiltonian

Throughout this work, we employ second-quantised electronic Hamiltonians, which are defined in Eq. (2) for a system of M electrons and K nuclei expressed in a basis of N spin orbitals [10]:

$$\hat{H} = \sum_{i,j}^N h_{ij} \hat{a}_i^\dagger \hat{a}_j + \frac{1}{2} \sum_{p,q,r,s}^N h_{pqrs} \hat{a}_p^\dagger \hat{a}_q^\dagger \hat{a}_r \hat{a}_s \equiv \sum_k^\Gamma \hat{H}_k . \quad (2)$$

\hat{a}_i^\dagger and \hat{a}_i denote the fermionic creation and annihilation operators, respectively. The one- and two-electron integrals h_{ij} and h_{pqrs} are defined as in Ref. [9] in the below equations:

$$h_{ij} = \int \chi_i^*(\mathbf{x}) \left(-\frac{1}{2} \nabla^2 - \sum_A^K \frac{Z_A}{r_{\mathbf{x},A}} \right) \chi_j(\mathbf{x}) \, \mathrm{d}\mathbf{x}, \quad (3)$$

$$h_{pqrs} = \int \frac{\chi_p^*(\mathbf{x}_1) \chi_q^*(\mathbf{x}_2) \chi_r(\mathbf{x}_2) \chi_s(\mathbf{x}_1)}{r_{1,2}} \, \mathrm{d}\mathbf{x}_1 \mathrm{d}\mathbf{x}_2 . \quad (4)$$

The set of functions $\{\chi_i(\mathbf{x})\}_{i=1}^N$ denote the spin orbitals, $r_{\mathbf{x},A}$ denotes the distance between the electron and the A 'th nucleus, and r_{12} the distance between two electrons. The charge of nucleus A is defined as Z_A , and $\mathbf{x} = (\mathbf{r}, \sigma)$ is a vector of the spatial coordinate \mathbf{r} and spin σ of an electron. The spin orbitals are obtained as a product of orthonormal spatial orbital functions $\{\Phi_i(\mathbf{r})\}_{i=1}^{N/2}$, spatial orbitals in short, and a spin-function $s(\sigma)$ which assigns either α or β spin to a spin orbital

$$\chi_i(\mathbf{x}) = \Phi_i(\mathbf{r}) s_i(\sigma). \quad (5)$$

The spatial orbitals are obtained from the linear combination of atom-centered spatial functions $\{\phi_\mu(\mathbf{r})\}_{\mu=1}^{N/2}$,

$$\Phi_i = \left(\sum_{\mu=1}^{N/2} C_{i,\mu} \phi_\mu(\mathbf{r}) \right), \quad (6)$$

where the elements $C_{i,\mu}$ of the coefficient matrix \mathbf{C} are the spatial orbital coefficients and store the contribution of each atom-centered spatial function $\phi_\mu(\mathbf{r})$ to the spatial orbital Φ_i .

Throughout this work, two representations of the Hamiltonian terms \hat{H}_k in Eq. (2) are employed: (i) a fermionic, and (ii) a qubit representation. The fermionic Hamiltonian representation of the terms is denoted

$$\hat{H}_k = h_k \hat{F}_k, \quad (7)$$

where

$$\hat{F}_k \in \begin{cases} a_i^\dagger a_i \\ a_i^\dagger a_j + a_j^\dagger a_i \\ a_p^\dagger a_q^\dagger a_q a_p \\ a_p^\dagger a_q^\dagger a_q a_r + a_r^\dagger a_q^\dagger a_q a_p \\ a_p^\dagger a_q^\dagger a_r a_s + a_s^\dagger a_r^\dagger a_q a_p \end{cases}. \quad (8)$$

It is directly obtained from the second-quantised Hamiltonian in Eq. (2) [9] by rearranging the two-body terms, employing the anti-commutation relations of fermionic operators [10]:

$$h_{pqrs} \hat{a}_p^\dagger \hat{a}_q^\dagger \hat{a}_r \hat{a}_s + h_{qpsr} \hat{a}_q^\dagger \hat{a}_p^\dagger \hat{a}_s \hat{a}_r = (h_{pqrs} + h_{qpsr}) \hat{a}_p^\dagger \hat{a}_q^\dagger \hat{a}_r \hat{a}_s. \quad (9)$$

Then, two-body terms involving all-up or all-down spin orbitals, i.e. $\sigma(p) = \sigma(q) = \sigma(r) = \sigma(s) \in \{\alpha, \beta\}$, are sorted,

$$\begin{aligned} & (h_{pqrs} + h_{qpsr}) \hat{a}_p^\dagger \hat{a}_q^\dagger \hat{a}_r \hat{a}_s + (h_{pqsr} + h_{qprs}) \hat{a}_p^\dagger \hat{a}_q^\dagger \hat{a}_s \hat{a}_r \\ &= (h_{pqrs} + h_{qpsr} - (h_{pqsr} + h_{qprs})) \hat{a}_p^\dagger \hat{a}_q^\dagger \hat{a}_r \hat{a}_s. \end{aligned} \quad (10)$$

Finally, non-hermitian terms, such as $h_{ij} \hat{a}_i^\dagger \hat{a}_j$, are joined with their hermitian conjugate counterpart to obtain the \hat{F}_k in Eq. (8). By contrast, the qubit Hamiltonian representation $\hat{H}_k = h_k \hat{P}_k$ is obtained by applying a fermion-to-qubit mapping to the fermionic operators in Eq. (2). Operators \hat{P}_k denote Pauli strings, which are Hermitian and unitary operators corresponding to tensor products of the Pauli (and identity) matrices.

Quantum circuit mappings are known for the unitary operators $\exp(-ih_k \hat{P}_k t)$ required for trotterised simulation with a qubit Hamiltonian [30], as well as the operators $\exp(-ih_k \hat{F}_k t)$ required for trotterised simulation with a fermionic Hamiltonian representation. The fermionic Hamiltonian exponentials can either be approximated by applying a fermion-to-qubit mapping to the operators \hat{F}_k [9, 30], and performing trotterised time evolution of the operator $\exp(-ih_k \hat{F}_k t)$. Alternatively, trotterised simulation with the employed fermionic Hamiltonian representation could be implemented exactly by utilising fermionic swap networks [60]. Arbitrary spin orbitals p and q (for one-body fermionic operators \hat{F}_k), or p, q, r, s (for two-body fermionic operators \hat{F}_k) can be brought to neighbouring qubits by layers of fermionic swap gates. The time evolution operators $\exp(-ih_k \hat{F}_k t)$ can then be exactly implemented as 2-local, or 4-local qubit unitaries.

We note that more efficient quantum circuit mappings of a fermionic Hamiltonian representation are achievable by factorisation of the electron repulsion integral tensor [12, 61, 62] compared to the fermionic representation we employed in this article. The focus

in this work is, however, on the assessment of different strategies, which employ orbital transformations in the context of trotterised Hamiltonian simulation. The strategies that we investigate should therefore be generally applicable, independent of the chosen Hamiltonian representation. As such, the simple fermionic Hamiltonian representation described above was employed for convenience.

2.2. Orbital transformations

The orbital basis, in which the second-quantised Hamiltonian in Eq. (2) is expressed, can be transformed by unitary transformations U_R , which we refer to as orbital transformations hereafter. The eigenspectrum of the electronic Hamiltonian is invariant under these orbital transformations.

Orbital basis transformations can be realised by transformations of the spatial orbital coefficient matrix \mathbf{C} (see Eq. (6) for the definition of the matrix elements of \mathbf{C}) as

$$\tilde{\mathbf{C}} = U_R \mathbf{C}. \quad (11)$$

Following Ref. [12], arbitrary orbital transformations can be constructed as products of Givens rotations:

$$U_R = \prod_{p < q}^{N/2} U_{R,\text{Givens}}(p, q). \quad (12)$$

In Eq. (12), Givens rotations $U_{R,\text{Givens}}(p, q)$ are defined as unitary transformations that implement a pair-wise rotation between the two spatial orbitals at indices p and q . The elements $\tilde{C}_{i,\mu}$ of the transformed coefficient matrix $\tilde{\mathbf{C}}$ resulting from the transformation of the coefficient matrix \mathbf{C} by Eq. (11) with $U_R = U_{R,\text{Givens}}(p, q)$ are:

$$\begin{aligned} \tilde{C}_{p,\mu} &= \cos(\theta_{pq})C_{p,\mu} - \sin(\theta_{pq})C_{q,\mu} \\ \tilde{C}_{q,\mu} &= \sin(\theta_{pq})C_{p,\mu} + \cos(\theta_{pq})C_{q,\mu} \\ \tilde{C}_{k \neq (p,q),\mu} &= C_{k,\mu}, \end{aligned} \quad (13)$$

where $\theta_{pq} \in [0, 2\pi)$ denotes the Givens rotation angle. The transformed coefficient matrix $\tilde{\mathbf{C}}$ defines a set of transformed orthonormal spatial orbitals $\{\tilde{\Phi}_i(\mathbf{r})\}_{i=1}^{N/2}$:

$$\tilde{\Phi}_i = \left(\sum_{\mu=1}^{N/2} \tilde{C}_{i,\mu} \phi_{\mu}(\mathbf{r}) \right), \quad (14)$$

which differs from the set of spatial orbitals defined in Eq. (6). Constructing the set of transformed spin orbitals $\{\tilde{\chi}_i(\mathbf{r})\}_{i=1}^{N/2}$ via Eq. (5) leads to transformed one- and two-body integrals \tilde{h}_{ij} and \tilde{h}_{pqrs} from Eqs. (3) and (4). The second-quantised Hamiltonian in the transformed basis is then given by

$$\tilde{\hat{H}} = \sum_{i,j}^N \tilde{h}_{ij} \tilde{a}_i^\dagger \tilde{a}_j + \frac{1}{2} \sum_{p,q,r,s}^N \tilde{h}_{pqrs} \tilde{a}_p^\dagger \tilde{a}_q^\dagger \tilde{a}_r \tilde{a}_s, \quad (15)$$

where \tilde{a}_i^\dagger and \tilde{a}_i denote creation and annihilation operators in the transformed orbital basis, respectively.

Alternatively, the transformation of the second-quantised Hamiltonian can be realised by transforming the creation and annihilation operators from the initial basis $(\hat{a}_p^\dagger, \hat{a}_q)$ to the transformed basis $(\tilde{a}_p^\dagger, \tilde{a}_q)$. As described in Ref. [10], a unitary transformation matrix

$$U_R = \exp(-\kappa) , \quad (16)$$

obtained as the exponential of the matrix representation κ of an anti-hermitian operator $\hat{\kappa} = -\hat{\kappa}^\dagger$, transforms the creation and annihilation operators as

$$\begin{aligned} \tilde{a}_p^\dagger &= \exp(-\hat{\kappa}) \hat{a}_p^\dagger \exp(\hat{\kappa}) \\ \tilde{a}_p &= \exp(-\hat{\kappa}) \hat{a}_p \exp(\hat{\kappa}) . \end{aligned} \quad (17)$$

To construct the unitary transformation matrix U_R in Eq. (16) as $U_R = U_{R,\text{Givens}}(p, q)$ in the spin orbital basis, which is needed for a quantum hardware implementation, we employ the anti-hermitian operator

$$\hat{\kappa} = \hat{\kappa}_{pq} = \theta_{pq} \left((\hat{a}_{2p-1}^\dagger \hat{a}_{2q-1} - \hat{a}_{2q-1}^\dagger \hat{a}_{2p-1}) + (\hat{a}_{2p}^\dagger \hat{a}_{2q} - \hat{a}_{2q}^\dagger \hat{a}_{2p}) \right) , \quad (18)$$

where we have mapped spatial orbitals at index p to index $2p - 1$ in the spin orbital basis for α spin orbitals and to index $2p$ for β spin orbitals. Inserting Eq. (18) into Eq. (16), the Givens rotation $U_{R,\text{Givens}}(p, q)$ expressed in the spin orbital basis is then obtained as:

$$U_{R,\text{Givens}}(p, q) = \exp(-\theta_{pq} (\hat{a}_{2p-1}^\dagger \hat{a}_{2q-1} - \hat{a}_{2q-1}^\dagger \hat{a}_{2p-1})) \cdot \exp(-\theta_{pq} (\hat{a}_{2p}^\dagger \hat{a}_{2q} - \hat{a}_{2q}^\dagger \hat{a}_{2p})) . \quad (19)$$

By expressing the unitary transformation matrix U_R in the spin orbital basis via Eqs. (12) and (19), the second-quantised Hamiltonian defined in Eq. (2) can be directly transformed as

$$U_R \hat{H} U_R^\dagger = \tilde{\hat{H}} . \quad (20)$$

With known quantum circuit decompositions for $U_{R,\text{Givens}}(p, q)$ [63], we can hence implement any orbital transformation unitary U_R on a quantum device.

2.3. Trotter error

Trotter error describes the error incurred in the approximation of the unitary operator $U = \exp(-i\hat{H}t)$ with the trotterised propagator

$$U_{\text{Trotter}} = \prod_{k=1}^{\Gamma} \exp(-i\hat{H}_k t) \equiv \exp(-i\hat{H}_{\text{eff}} t) . \quad (21)$$

In Eq. (21), U_{Trotter} is constructed from a first-order Trotter formula, which we consistently employ hereafter. Trotterised time evolution effectively corresponds to the exact Hamiltonian simulation of the effective Hamiltonian $\hat{H}_{\text{eff}} = -\ln U_{\text{Trotter}}/(it)$. Trotter error can be quantified in various ways, (i) as the difference in the propagator [44]

$$\Delta U(t) = e^{-i\hat{H}_{\text{eff}} t} - e^{-i\hat{H} t} , \quad (22)$$

(ii) as differences in the operator spectrum, such as a difference in the ground state energies,

$$\Delta E_0 = E_{0,\text{Trotter}} - E_0 , \quad (23)$$

(iii) as the difference in the time-evolved Hilbert-space state vectors, measured, for example, as their L^2 -norm,

$$|\Delta_{|\psi\rangle}| = |e^{-i\hat{H}t} |\psi\rangle - e^{-i\hat{H}_{\text{eff}} t} |\psi\rangle| , \quad (24)$$

(iv) as a fidelity measure[64], which is based on the time-evolving overlap of the true state with the one generated by \hat{H}_{eff} ,

$$f(t) = 1 - \langle \psi(t) | \psi_{\text{Trotter}}(t) \rangle = 1 - \langle U(t) \psi(0) | U_{\text{Trotter}}(t) \psi(0) \rangle , \quad (25)$$

(v) or to an offset in the autocorrelation function (ACF),

$$g(t) = |\langle \psi(0) | \psi(t) \rangle - \langle \psi(0) | \psi(t, \text{Trotter}) \rangle|. \quad (26)$$

We expect the ACF offset $g(t)$ to be strongly correlated with the Trotter error in the ground state, because the ACF $\langle \psi(t) | \psi(0) \rangle$ with $|\psi(0)\rangle = |\psi_0\rangle$ corresponds to a cosine wave that oscillates with period $2\pi/E_0$. We note that upper bounds for the norm of the difference in the propagated wave function, as defined in Eq. (24), have recently been derived [65]. Since their calculation is computationally demanding, we did not evaluate them in this work. We refer to Ref. [66] for a discussion of the relation between fidelity and operator norm errors. In this work, unless otherwise noted, we measure Trotter error by ΔE_0 and refer specifically to the absolute difference $|\Delta E_0|$ in the ground state energy of \hat{H} and \hat{H}_{eff} .

2.3.1. Analytical error expressions of the propagator and its spectrum

While critical for the development of accuracy-guaranteed protocols, operator spectral norms make the worst-case assumption $\|A\|_2 = \sup_{|\vec{v}|=1} |A\vec{v}|$, where A denotes an arbitrary bounded operator which acts on elements $\vec{v} \in \mathcal{H}$ of a finite-dimensional Hilbert space \mathcal{H} . For a Trotter step number s in a Hamiltonian simulation with a guaranteed Trotter error below a targeted accuracy, an upper bound on $|\Delta E_0|$ is required. Lemmata 3 and 4 in the supplementary information of Ref. [11] establish the relation

$$\|\Delta U(t)\|_2 \leq t\gamma(t) \Rightarrow \|\hat{H} - \hat{H}_{\text{eff}}\|_2 \leq \gamma(t) \Rightarrow |\Delta E_0| \leq \gamma(t) \quad (27)$$

between ground-state-energy Trotter error and the spectral norm of the propagator difference $\|\Delta U(t)\|_2$ under the assumption that $\gamma(t)$ is a non-decreasing function on the interval $[0, \infty)$. The currently tightest bounds on $\|\Delta U(t)\|_2$, which apply to a general non-sparse Hamiltonian, were derived by Childs et al. [44] for a first-order Trotter formula decomposition,

$$\|\Delta U(t)\|_2 \leq \frac{t^2}{2}\alpha \quad (28)$$

with

$$\alpha = \sum_{a=1}^{\Gamma} \left\| \sum_{b>a}^{\Gamma} [\hat{H}_b, \hat{H}_a] \right\|_2. \quad (29)$$

Accuracy-guaranteed protocols are known to overestimate the required Trotter numbers n by multiple orders of magnitude for electronic Hamiltonians [11, 27, 31, 67]. If the Trotter error is evaluated based on the norm of the propagator difference, this can, for instance, lead to an incorrect assessment of low-Trotter-error Hamiltonian partitionings, as demonstrated in Refs. [12, 27]. Since the determination of a consistently low Trotter error orbital basis requires a qualitatively correct numerical comparison of $|\Delta E_0|$ across multiple orbital basis, we require an alternative approximation of the ground-state-energy Trotter error, rather than upper bounds on Trotter error.

Estimates on ground-state-energy Trotter error from time-independent perturbation theory have previously been utilised for this purpose [31]. Expressions have been derived for first- [68] and second-order [46] Trotter formulae of Hamiltonians in Eq. (2) with an arbitrary number of terms Γ . These expressions derive the leading order term of the effective Hamiltonian \hat{H}_{eff} by recursive application of the Baker-Campbell-Hausdorff formula.

For the first-order Trotter formula, the energy error estimate $|\Delta E_{\text{PT}}|$, derived in the preprint [68], reads:

$$\begin{aligned} |\Delta E_{\text{PT}}| &= |\langle \psi_0 | \hat{H} - \hat{H}_{\text{eff}} | \psi_0 \rangle| \\ &= |\langle \psi_0 | \hat{v}_2 | \psi_0 \rangle| t^2 + \sum_{n>0} \frac{|\langle \psi_n | \hat{V}_1 | \psi_0 \rangle|^2}{E_0 - E_n} t^2 + O(t^3) \end{aligned} \quad (30)$$

with

$$\begin{aligned} \hat{V}_1 &= -\frac{i}{2} \sum_{a=1}^{\Gamma-1} \sum_{b=a+1}^{\Gamma} [\hat{H}_b, \hat{H}_a], \\ \hat{v}_2 &= -\frac{1}{3} \sum_{a=1}^{\Gamma-1} \sum_{b=a+1}^{\Gamma} \sum_{c=b}^{\Gamma} \left(1 - \frac{\delta_{bc}}{2}\right) [\hat{H}_c, [\hat{H}_b, \hat{H}_a]]. \end{aligned} \quad (31)$$

Note that the calculation of $|\Delta E_{\text{PT}}|$ in Eq. (30) is even more cumbersome compared to ΔE_0 , since it requires knowledge of the entire set of eigenvalues E_n and eigenvectors $|\psi_n\rangle$ of the Hamiltonian \hat{H} . Ref. [27] finds the first and second terms in Eq. (30) to be correlated. For our analysis of Trotter error for larger molecular systems, we require a quantity that can be easily calculated and that correlates with $|\Delta E_0|$. Accordingly, we target

$$\epsilon_2 = |\langle \psi_0 | \hat{v}_2 | \psi_0 \rangle| \quad (32)$$

as a time-independent error estimate from perturbation theory. Then, $\epsilon_2 t^2$ allows for a comparison with the exact Trotter error for given times t . In case of poor correlation, an approximation of the second sum in Eq. (30) can always be added as a correction. However, based on our results, this does not appear to be necessary for the molecular systems considered in this work.

2.4. Descriptors correlating with Trotter error

Analytical expressions of Trotter error that are straightforwardly interpretable in terms of the effect of the orbital basis are given in Eqs. (29) and (30). But, both equations comprise (nested) commutators of the Hamiltonian terms \hat{H}_k and are therefore not straightforward to evaluate. However, these equations suggest that the following three descriptors, which depend only on the orbital basis and are easier to evaluate, may be sufficient to assess Trotter error: (i) the number of non-negligible coefficient terms Γ (because having fewer terms contribute to the (nested) commutator sum should decrease α and $\|\hat{v}_2\|_2$), where we will define a term \hat{H}_k as non-negligible, if it features a coefficient weight $|h_k| \leq 10^{-8} E_h$, (ii) the coefficient weights $|h_k|$, which are determined for a fermionic Hamiltonian representation by Eqs. (8)-(10) and for a qubit Hamiltonian depend on the employed fermion-to-qubit mapping applied to the operators in Eq. (2), and (iii) the distribution of the Configuration Interaction (CI) coefficients in the linear combination of Slater determinants of the ground-state wave function $|\psi_0\rangle$.

Following Eqs. (11)-(15), it is apparent that orbital transformations affect the entire set of one- and two-electron integrals. As described in section 2.1, the one- and two-electron integrals determine the weights h_k of the terms \hat{H}_k in the Hamiltonian. Hence, since the weights $|h_k|$ cannot be minimised independently, one can resort to minimising their sum $\lambda = \sum_k |h_k|$, which is usually called the 1-norm for a qubit Hamiltonian representation [37, 55, 56]. In general, we will denote the ‘1-norm’ as λ_F for a fermionic Hamiltonian and as λ_Q for a qubit Hamiltonian. The relation between upper bounds on Trotter error in the propagator difference norm and the respective 1-norm can be emphasised by deriving an

upper bound on α in Eq. (29). An upper bound $\alpha' \geq \alpha$ that is directly proportional to λ_F^2 or λ_O^2 is derived in the Supporting Information (SI).

The influence of the ground state wave function $|\psi_0\rangle$ on Trotter error is evident from Eq. (30). In particular, the multi-reference character of the ground state wave function might be of relevance for Trotter error. This could explain prior findings in Ref. [31] that local orbital bases incur large Trotter errors since $|\psi_0\rangle$ in a local orbital bases can have notable strong multi-reference character compared to the canonical basis. Data for our investigated systems which support this claim can be found in the SI.

2.5. Construction of randomised bases and series order propagators

In this work, we specifically employ propagators, which change the orbital basis between Trotter steps. In trotterised Hamiltonian simulations with a factorised, fermionic Hamiltonian representation [12], the orbital basis is transformed within a Trotter step. For our investigation of the effect of random orbital basis transformations during trotterised Hamiltonian simulation, changing the orbital basis between Trotter steps appears preferable: it straightforwardly ensures that each term \hat{H}_k is applied in each Trotter step. Additionally, fewer orbital transformation unitaries U_R are required, if the basis is transformed between Trotter steps instead of (multiple times) inside each Trotter step. We review the randomised series reordering propagator introduced by Childs et al. in Ref. [54] below. It matches the one in Ref. [69] for a fixed time t per Trotter step.

Starting from the exact propagator U for a given time t defined in Eq. (1), the time evolution is split into η sub-steps, each evolving the system for equal time $t_n = t/\eta$

$$U = \prod_{n=1}^{\eta} \exp(-i\hat{H}t_n). \quad (33)$$

We now introduce a reordering operator $\mathcal{P}_{\vec{\sigma}}$, which acts on the Hamiltonian defined in Eq. (2) by reordering its Γ terms according to the elements of the reordering vector $\vec{\sigma}$. The vectors $\vec{\sigma} \in \mathbb{Z}^\Gamma$ are arrays of shuffled integers from 1 to Γ , containing each integer exactly once. Due to the associativity of operator addition, we can therefore insert a different reordering operator $\mathcal{P}_{\vec{\sigma}_n}$ at each time evolution step n into Eq. (33) to arrive at the exact expression

$$U = \prod_n \exp(-i\mathcal{P}_{\vec{\sigma}_n} \hat{H} t_n). \quad (34)$$

After Trotterisation of the exponential operator, Eq. (35) is obtained. The ordering of the terms in the Hamiltonian now affects the resulting propagator [47] and hence the spectrum of the effective Hamiltonian

$$U_{\text{reo}} = \prod_n \prod_k^{\Gamma} \exp(-i\hat{H}_{k(\vec{\sigma}_n)} t_n). \quad (35)$$

To emphasise the dependence of the term index k on the explicit reordering in each step n , we mark the index k as being functionally dependent on the reordering vector $\vec{\sigma}_n$.

Analogously, the derivation of the trotterised orbital basis rotation propagator U_{rot} also starts from Eq. (33). We begin by inserting the identity operator $\mathcal{I} = U_{R,n}^\dagger U_{R,n}$ to obtain

$$U = \prod_n U_{R,n}^\dagger U_{R,n} \exp(-i\hat{H}t_n) U_{R,n}^\dagger U_{R,n}. \quad (36)$$

The orbital transformations $U_{R,n}$ expressed in the spin orbital basis are defined here following Eqs. (12) and (19). The subscript n again denotes that the orbital transformations may vary from time evolution step to time evolution step. Inserting the identity

$$\exp(U_R \hat{H} U_R^\dagger) = U_R \exp(\hat{H}) U_R^\dagger \quad (37)$$

into Eq. (36), we arrive at the expression

$$U = \prod_n U_{R,n}^\dagger \exp(-i U_{R,n} \hat{H} U_{R,n}^\dagger t_n) U_{R,n}. \quad (38)$$

With Eq. (20), we then obtain the exact propagator

$$U = \prod_n U_{R,n}^\dagger \exp(-i \tilde{H}^{(n)} t_n) U_{R,n}, \quad (39)$$

where $\tilde{H}^{(n)}$ denotes the second-quantised Hamiltonian in the respective orbital basis of the n 'th time evolution step. The trotterised propagator, which may become subject to benefit from error cancellation effects induced by a transformation of the orbital basis, is finally obtained as

$$U_{\text{rot}} = \prod_n U_{R,n}^\dagger \left(\prod_k^\Gamma \exp(-i \tilde{H}_k^{(n)} t_n) \right) U_{R,n}. \quad (40)$$

We employ the following notation to differentiate between the ' η -basis-propagators' U_{rot} and the ' η -ordering-propagators' U_{reo} , and their 'constituent' propagators, $U_{\text{rot},n}$ and $U_{\text{reo},n}$:

$$U_{\text{rot}} = \prod_n U_{R,n}^\dagger U_{\text{rot},n} U_{R,n} \quad (41)$$

with

$$U_{\text{rot},n} = \prod_k^\Gamma \exp(-i \tilde{H}_k^{(n)} t_n), \quad (42)$$

and

$$U_{\text{reo}} = \prod_n U_{\text{reo},n} \quad (43)$$

with

$$U_{\text{reo},n} = \prod_k^\Gamma \exp(-i \hat{H}_{k(\vec{\sigma}_n)} t_n). \quad (44)$$

The propagators U_{rot} and U_{reo} evolve the wave function for a total time t , whereas the constituent propagators $U_{\text{rot},n}$ and $U_{\text{reo},n}$ evolve the wave function for a time step t_n .

Additionally, $\vec{\theta}$ will be used as a short-hand notation for the Givens rotation representation of the orbital-basis unitary transformations U_R as defined in Eq. (12). The elements of the vector $\vec{\theta} \in \mathbb{R}^{(\frac{N}{2}(\frac{N}{2}-1))/2}$ list the coefficients θ_{pq} of the individual Givens rotations $U_{R,\text{Givens}}(p, q)$ (see Eq. (19)) from which U_R is constructed. We employ the canonical orbital basis as the reference basis which defines the zero-vector $\vec{\theta} = \vec{0}$.

We finally note that in the context of Hamiltonian simulation for a time t_{total} , the η -basis-propagators and η -ordering-propagators introduced in this section are akin to periodically driven quantum systems [70]. This is because in Eq. (41) and (43) we defined that U_{rot} and U_{reo} evolve the wave function for a total time t , which is the time evolution associated with a single Trotter step and not the total time evolution t_{total} of Hamiltonian simulation (see Eq. (1)). A Hamiltonian simulation of time t_{total} with a Trotter step number s as defined by Eq. (1) corresponds to a trotterised simulation with a Trotter step number $s \cdot \eta$, where the orbital basis is changed every Trotter step if an η -basis-propagator is employed. If the same η -basis propagator is continuously applied, the orbital basis changes

periodically (with a period of η Trotter steps) throughout the Hamiltonian simulation. To obtain randomised propagators which randomly vary the orbital basis each Trotter step hence requires the choice of a Trotter step number $s = 1$, based on the definitions employed throughout this work. This brief excursion to periodically driven quantum systems hence highlights that the idea to utilise ‘modulation schemes’ such that the simulated effective Hamiltonians reproduce exact Hamiltonian simulation more accurately [71] is not unique to randomised propagator constructions.

3. Computational methodology

All Cartesian coordinates of the molecular structures were taken from PubChem [72], with the exception the cyclobutadiene (CBD) molecule, whose structure we optimised within a Kohn-Sham DFT calculation with the `geomeTRIC` library [73] using the B3LYP exchange-correlation energy functional [74] and a cc-pVTZ basis set [75].

For the few-atomic systems investigated in section 4.1, we chose the minimal sto-3g basis set [76] to obtain results, which can be compared to those in Ref. [31]. Active spaces are chosen around the Fermi level when employing a canonical orbital basis. For restricted MP2 (RMP2) natural orbitals, the equivalent to the Fermi level is placed at the threshold, where the spatial orbital occupancy drops sharply from close to two (occupied orbitals) to close to zero (virtual orbitals). These active spaces contain all orbitals except the frozen core orbitals. The number of electrons in the active space relates to the number of occupied Hartree-Fock or RMP2 orbitals, assigning all other orbitals in the active space to the virtual orbital space; the resulting active spaces are listed in Table 1.

For small molecular π -systems, we employed the cc-pVTZ basis set [75], for the π -system of octatetraene and larger ones the cc-pVDZ basis set [75] was employed. The active space spatial orbitals corresponding to the π -orbitals were selected manually as follows: For π -systems with $N/4$ conjugated π bonds, the selected active spaces of $N/2$ spatial orbitals and $M = N/2$ electrons include $N/4$ spatial orbitals that are occupied in the HF (or RMP2 natural orbital) reference wave function and $N/4$ spatial orbitals from the virtual space. The selected occupied orbitals were visually identified as π -bonding orbitals and the virtual orbitals as their anti-bonding counterparts. For the pyrrole molecule with $N/4 = 2$ conjugated π -bonds, an additional spatial orbital from the occupied space that corresponded to a p_z -type orbital was added to the active space. Exact details on the employed active spaces are provided in the Zenodo repository that accompanies this work.

Orbital localisations were carried out with the Foster-Boys scheme [77] as implemented in PySCF [78]. Restricted MP2 (RMP2) natural orbitals were obtained with PySCF. As an example, π -orbitals in different bases are shown for butadiene and naphthalene in the SI.

The second-quantised electronic Hamiltonian was obtained in a spin orbital basis with the function ‘`qchem.fermionic_observable`’ implemented in the PennyLane python library [79]. The one- and two-electron integrals were calculated with PySCF. As previously described in section 2.4, we neglected all terms \hat{H}_k with coefficient weights $|h_k|$ below $10^{-8} E_h$. The qubit Hamiltonian was obtained by Jordan-Wigner mapping [80] of the electronic Hamiltonian, as implemented in PennyLane.

Two orderings of the Trotter series were employed in this work: (i) a magnitude ordering [47], where the terms \hat{H}_k were ordered by decreasing $|h_k|$ to incur consistently low Trotter error independent of the orbital basis, and (ii) index-dependent orderings for fermionic and qubit Hamiltonian representations, which facilitate the evaluation of the effect of orbital transformations on Trotter error with fixed Trotter series-orderings. Details on utilised index-dependent orderings are provided in the SI.

The exact Trotter energy error was calculated in two ways: up to (but excluding) section

4.3 ΔE_0 was calculated by inverse Fourier transform (IFT) of the ACF as

$$\Delta E_0 = E_0(\epsilon) - E_{0,\text{Trotter}}(\epsilon), \quad (45)$$

where

$$E_0(\epsilon) = \min(\text{IFT}(\langle\langle\psi_0|\psi(t)\rangle\rangle)) \quad (46)$$

and

$$E_{0,\text{Trotter}}(\epsilon) = \min(\text{IFT}(\langle\langle\psi_0|\psi_{\text{Trotter}}(t)\rangle\rangle)) \quad (47)$$

with $|\psi(t)\rangle$ and $|\psi_{\text{Trotter}}(t)\rangle$ defined in Eq. (25). Eigenenergies of the Hamiltonian by IFT of the ACF can only be obtained up to precision ϵ , depending on the total time evolution length t_{total} .

For a comparison of Trotter errors of η -basis-propagators and η -ordering-propagators (Eqs. (41) and (43)) and their individual constituents (Eqs. (42) and (44)), we employed a second, more convenient approach, where we calculated Trotter error ΔE_0 by diagonalisation of the spin-orbital matrix representation of the effective Hamiltonian \hat{H}_{eff} directly, as defined in Eq. (21). This is beneficial as we were not restricted with respect to the precision ϵ with which we would obtain E_0 and $E_{0,\text{Trotter}}$ due to a finite-length ACF.

The ground state wave function $|\psi_0\rangle$ was obtained from Density Matrix Renormalization Group (DMRG)-CI calculations with the QCMAquis computer program [81] for a bond dimension of 1024. To map the ground-state matrix-product-state wave function to a sum of occupation number vectors in the determinantal basis, we exploited the SR-CAS algorithm [82] as implemented in QCMAquis [81].

Our construction of the trotterised and exact propagators $U_{\text{Trotter}}(t)$ and $U(t)$, respectively, utilised the PennyLane [79], OpenFermion [83], and scipy [84] libraries. Parts of the trotterised propagator construction utilise the code repository [85] of Ref. [27]. Unless otherwise noted, Trotter step numbers were chosen such that $t = 0.95\pi/|E_0|$. This choice of step size assured that we were using the maximum possible step size while adhering to the Nyquist-Shannon sampling theorem [86] for the Fourier transformation. The factor of 0.95 guarantees that the signal $E_{0,\text{Trotter}}$ will not be cut off in the spectrum if $E_{0,\text{Trotter}}$ is smaller than E_0 . We refer to Table 1 for an overview of the resulting times t for the systems considered in this work.

A python program was written for the calculation of the upper bound of the Trotter error α and for the perturbative error estimate ϵ_2 (according to Eq. (29) and Eq. (32), respectively).

For commutator elements of the fermionic Hamiltonian representation, we calculated $[\hat{F}_b, \hat{F}_a]$ with an in-house program by implementing the analytical results of the commutators between normal-ordered one- to three-electron terms (see the SI for explicit expressions). For commutator elements of the qubit Hamiltonian representation, the PennyLane library was exploited to calculate commutators of Pauli strings.

Moreover, the calculation of ϵ_2 requires the evaluation of up to four-electron operator matrix elements. We used QCMAquis [81] to calculate the unique elements of all non-zero one-body to four-body reduced density matrices (one- to 4-RDMs) in the spin orbital basis. Obviously, the calculation of 4-RDMs is expensive due to the number of elements, scaling with the number of active space orbitals as N^8 . This steep scaling creates a natural restriction to up to 10 spatial orbitals (20 spin orbitals, and hence 20 qubits) to calculate estimates of the Trotter energy error ϵ_2 . Even for the 10 spatial orbital case, owing to the sheer number of terms in the Hamiltonian \hat{H}_k , calculating the double commutator sum \hat{v}_2 is very expensive despite the calculation of \hat{v}_2 in Eq. (31) being embarrassingly parallel.

Calculating ϵ_2 for a qubit Hamiltonian representation required the double commutator sum of Pauli strings to be evaluated. Afterwards, we employed the reverse Jordan-Wigner

mapping implemented in OpenFermion [83] to map the resulting sum of Pauli strings to a sum of normal-ordered fermionic operators. The previously calculated one- to four-body RDM elements were then exploited to calculate ϵ_2 .

We calculated the fidelity error $f(t)$ and the autocorrelation function offset $g(t)$ after a single time step with $t = 0.95\pi/|E_0|$. We observed the best correlations with exact-error calculations after a single step, when compared to calculations after multiple time steps. The calculation of $f(t)$ and $g(t)$ was performed by the tangent-space time-dependent DMRG algorithm [87] as implemented in QCMAquis [81]. In a local QCMAquis version, the construction of the trotterised time evolution matrix product operators $e^{-ih_k\hat{F}_k t}$ was implemented.

Orbital transformations were obtained as products of Givens rotations following Eqs. (12) and (19) by direct transformation of creation and annihilation operators:

$$\begin{pmatrix} \tilde{a}_p^\dagger \\ \tilde{a}_q^\dagger \end{pmatrix} = \begin{pmatrix} \cos \theta_{pq} & -\sin \theta_{pq} \\ \sin \theta_{pq} & \cos \theta_{pq} \end{pmatrix} \begin{pmatrix} \hat{a}_p^\dagger \\ \hat{a}_q^\dagger \end{pmatrix} \quad (48)$$

and

$$\begin{pmatrix} \tilde{a}_p \\ \tilde{a}_q \end{pmatrix} = \begin{pmatrix} \cos \theta_{pq} & -\sin \theta_{pq} \\ \sin \theta_{pq} & \cos \theta_{pq} \end{pmatrix} \begin{pmatrix} \hat{a}_p \\ \hat{a}_q \end{pmatrix}. \quad (49)$$

Consequently, the creation and annihilation operators can be directly transformed to obtain $\tilde{\hat{H}}^{(n)}$ from $U_{R,n}$ and \hat{H} according to Eq. (20) without the explicit construction of the matrix $U_{R,n}$ in the spin orbital basis.

To allow for a straightforward comparison of Trotter error ΔE_0 of propagators U_{reo} and $U_{\text{reo},n}$ (as well as U_{rot} and $U_{\text{rot},n}$) obtained for different molecules, we normalised the spectra of their Hamiltonians and shifted them to the interval $[-1, 0]$.

All plots in this work were created with the matplotlib python package [88].

4. Results

In this section, we present results for the fermionic Hamiltonian representation, since it enabled the analysis of the additional estimates of Trotter error $f(t)$ and $g(t)$ (see Eqs. (25) and (26)) as described in section 3. The results for the qubit Hamiltonian representation are provided in the SI. However, a discussion of differences and similarities in the results obtained for the two different Hamiltonian representations has been included in this section. Section 4.1 discusses Trotter errors for atoms in various orbital bases similar to those in Ref. [31]. In section 4.2, we compare Trotter error for π -systems with up to six spatial orbitals in different orbital basis sets. We evaluate the correlation of Trotter error estimates αt^2 , $\epsilon_2 t^2$, $g(t)$ and $f(t)$ with exact ground state energy Trotter error $|\Delta E_0|$. For estimates which show notable correlation with Trotter error, we perform calculations on larger π -systems with active spaces of up to ten spatial orbitals. We report on the correlation of descriptors with Trotter error in 4.2.3. Randomised η -basis- and η -ordering-propagators (see Eqs. (41) and (43)) are discussed in section 4.3. Finally, we investigated whether the observed continuity of Trotter error as a function of the transformed orbital basis $\vec{\theta}$ allows for the determination of an orbital basis without a Trotter error by a bisection method in the SI.

4.1. Atomic, diatomic, and triatomic systems

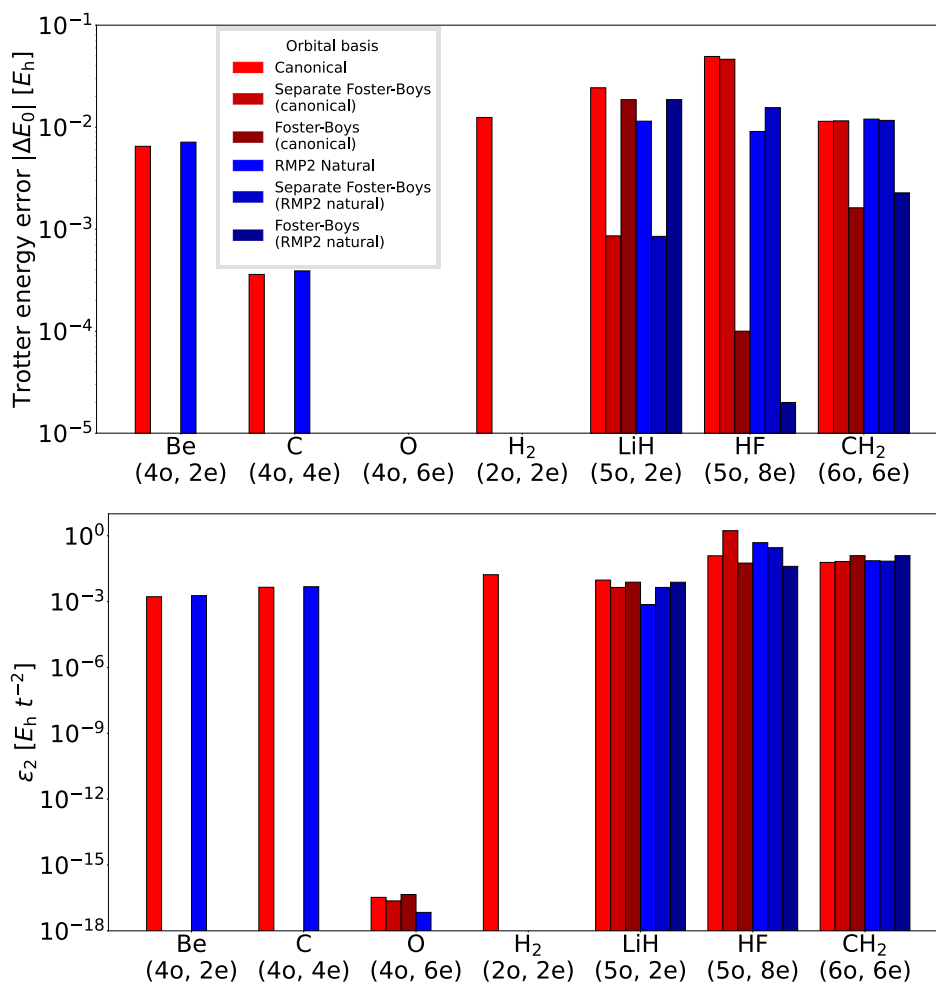


Figure 1: Top: Trotter energy errors $|\Delta E_0|$ obtained to precision $\epsilon = 10^{-5} E_h$ (see Eqs. (45)-(47)) in various common orbital bases. Bottom: perturbation theory energy error estimate ϵ_2 defined in Eq. (32). Results were obtained for small atomic systems in a sto-3g basis. For evolution times t per Trotter step see Table 1. The fermionic Hamiltonian representation and a magnitude ordering of the Trotter series were employed.

Fig. 1 shows how the Trotter energy error depends on the choice of orbital basis for small systems of denoted active space sizes. The following six orbital bases were considered: the canonical orbital basis, a separately localised orbital basis starting from canonical orbitals, and localised orbitals starting from canonical orbitals. The RMP2 natural orbital basis, a separately localised orbital basis starting from RMP2 natural orbitals, and localised orbitals starting from RMP2 natural orbitals. A separately localised canonical (or RMP2 natural) orbital basis refers to the orbital basis obtained from separate orbital localisation of the occupied and virtual orbitals in the canonical (or RMP2 natural) orbital basis active space. A localised canonical (or RMP2 natural) orbital basis refers to the orbital basis obtained from a single orbital localisation, which includes, and, hence, ‘mixes’ the occupied and virtual orbitals in the canonical (or RMP2 natural) orbital basis active space.

We have omitted (separately) localised orbital bases data from the plot for the few-atomic systems (Be, C, O, H₂), where the Foster-Boys orbital localisation was inapplicable (see the missing bars for the Be and C atom systems in Fig. 1 for example). For molecular hydrogen (H₂), the canonical and RMP2 natural orbitals are identical, which is why the

RMP2 natural orbital basis result is omitted in Fig. 1. Active spaces of $N/2$ spatial orbitals and M electrons are denoted as $(N/2o, Me)$. The evolution times t employed in the construction of $U_{\text{Trotter}}(t)$ are provided in Table 1.

Molecule	basis set	CAS orbitals	CAS electrons	CASCI energy [E_h]	Time per Trotter step t [E_h^{-1}]
Be atom	sto-3g	4	2	-0.978	3.051
C atom	sto-3g	4	4	-5.247	0.569
O atom	sto-3g	4	6	-15.367	0.194
H ₂	sto-3g	2	2	-1.851	1.612
LiH	sto-3g	5	2	-1.080	2.762
HF	sto-3g	5	8	-28.020	0.107
CH ₂	sto-3g	6	6	-10.659	0.28
butadiene (BD)	cc-pVTZ	4	4	-3.308	0.902
cyclobutadiene (CBD)	cc-pVTZ	4	4	-3.519	0.848
pyrrole (Pyrr)	cc-pVTZ	5	6	-7.044	0.424
hexatriene (Hexa)	cc-pVTZ	6	6	-5.834	0.512
benzene (Benz)	cc-pVTZ	6	6	-6.442	0.463
pyridine (Pyri)	cc-pVTZ	6	6	-6.756	0.442
octatetraene (Octa)	cc-pVDZ	8	8	-11.207	0.266
decapentaene (Deca)	cc-pVDZ	10	10	-11.671	0.256
naphthalene (Naph)	cc-pVDZ	10	10	-13.795	0.216

Table 1: Systems and their abbreviations in parentheses, their associated active space sizes (number of spatial orbitals $N/2$ and number of electrons M), and ground state energy E_0 of the Complete Active Space (CAS)-CI Hamiltonian for the RMP2 natural orbitals active space. The time evolution per Trotter step was determined as $t = 0.95\pi/|E_0|$. In case of ambiguity, the names for linear conjugated π -systems refer to the ‘all’ (E) isomer, that is, the IUPAC name for the selected octatetraene isomer would be $(3E,5E)$ -octa-1,3,5,7-tetraene.

The Trotter error $|\Delta E_0|$ for the oxygen atom is below the energy-resolution threshold of $\epsilon = 10^{-5} E_h$ for these calculations, and can hence not be shown in Fig. 1. The differing values of ϵ_2 for the oxygen atom are a result of numerical error, due to the very small values for $|\epsilon_2|$ which are below $10^{-16} E_h t^{-2}$.

It is obvious from Fig. 1 that the choice of orbital basis can significantly affect Trotter error. The most notable example is observed for the HF molecule, where the energy error $|\Delta E_0|$ incurred due to Trotterisation can vary by up to 3 orders of magnitude between different orbital bases. Similar results are observed for a qubit Hamiltonian representation which we provide in the SI. We note that when employing the qubit Hamiltonian representation, the Trotter error of the oxygen atom deviates notably less compared to the other systems.

Similar to Ref. [31], we find for a perturbative error estimate of Trotter error that the oxygen atom incurs a Trotter error, which is many orders of magnitude smaller compared to other investigated systems. We observe comparable results regarding the variation of a Trotter error estimate with the orbital basis choice to Ref. [31]. Namely, the difference in Trotter errors between different systems is of comparable magnitude, and the variance in error with different orbital choices are generally in agreement. Differences in our results are to be expected, given the use of a different order Trotter formula (first versus second order), different Trotter series-ordering (magnitude [47] versus lexicographic ordering [31, 58]) and slightly different active spaces (the core orbitals are frozen in our case, whereas

they are included in the active space in Ref. [31]).

Ref. [31] reported that the CASCI natural orbital basis or canonical basis lead to reduced Trotter error compared to a local basis in the majority of cases. We did not observe a clear trend which choice of orbital basis generally leads to the lowest Trotter errors, because of (i) the increased number of investigated orbital bases compared to Ref. [31] per molecule, and (ii) the limited number of available data points for localised bases of the atomic systems for which (Foster-Boys) orbital localisation is inapplicable.

4.2. π -conjugated molecules

We now investigate Trotter errors for a set of homologous molecules, where the effect of orbital localisation is more pronounced: orbital active spaces comprising the π -electrons in the π -systems. Based on the data tabulated in the SI, we found: (i) The difference between canonical and local basis (measured by differences in the 1-norm) for π -systems versus atomic systems is increased, (ii) the orbitals in π -system active spaces retain a consistent character with an increasing number of ethylene units, and (iii) the multi-reference character of $|\psi_0\rangle$ increases with the number of conjugated π bonds in these systems [89, 90], both for canonical and localised bases. Trotter energy errors $|\Delta E_0|$ for the π -systems with up to six spatial orbitals are shown in Fig. 2 (abbreviations of the names of the π -systems are defined in Table 1). For the CBD system, the separate Foster-Boys localisation, starting both from canonical and natural orbitals, did not converge. Hence, these data points were omitted in Fig. 2.

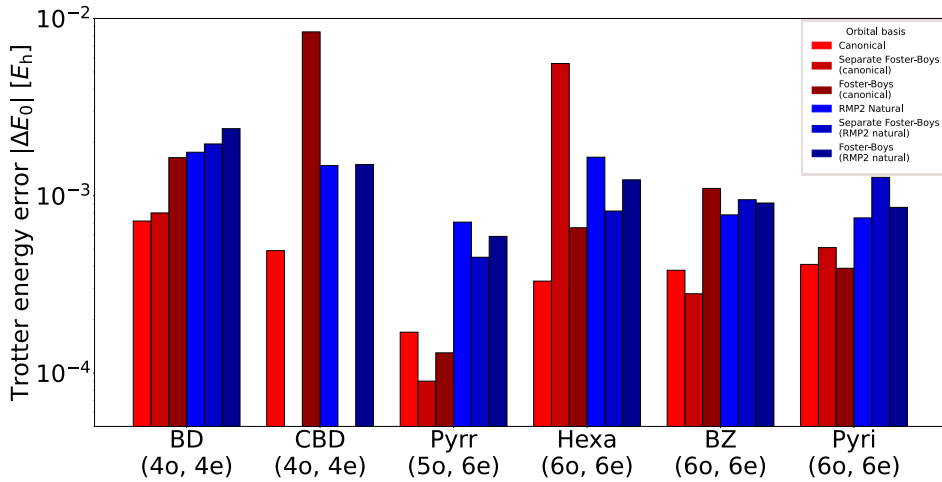


Figure 2: Trotter energy error $|\Delta E_0|$ obtained to precision $\epsilon = 10^{-5} E_h$ (see Eqs. (45)-(47)) for π -systems with active spaces of up to 6 spatial orbitals in various common orbital bases. The fermionic Hamiltonian representation and a magnitude ordering of the Trotter series were employed. For evolution times t per Trotter step and for the abbreviations of the different molecules, we refer to Table 1.

At most, up to an order of magnitude variance in Trotter error is observed for each system in Fig. 2. In most cases, Trotter errors for (localised) canonical orbitals are decreased compared to (localised) RMP2 natural orbitals. The decrease is minor and might simply be a consequence of the slightly smaller CASCI energies associated with the RMP2 orbital active spaces compared to the canonical orbital active spaces (see the SI for details). Results for the qubit Hamiltonian representation are shown in the SI. A similar variance of up to an order of magnitude in Trotter error is observed among the investigated orbital bases. The data does not suggest a consistent effect of orbital localisation on Trotter error.

4.2.1. Comparison of exact Trotter error and error estimates

We now study the correlation of $|\Delta E_0|$ and various estimates of Trotter error. For a direct comparison, we refer to Fig. 2 for data on $|\Delta E_0|$, Fig. 3 for $\epsilon_2 t^2$, $f(t)$ and $g(t)$, and to the SI for a plot of $\alpha t^2/2$. We measured correlations by the Pearson correlation coefficient R^2 between Trotter error $|\Delta E_0|$ and target error estimates, and considered all data points in the data set of π -systems displayed in Fig. 2, i.e. π -systems with up to six spatial orbitals. For $\epsilon_2 t^2$, $f(t)$, and $g(t)$ we found significant correlation, with R^2 values of 0.656, 0.557, and 0.818, respectively. However, poor correlation was observed with $\alpha t^2/2$ ($R^2 = 0.078$). Accordingly, the perturbative error estimate $\epsilon_2 t^2$ as well as the error measures in the time-evolved wave function $f(t)$ and $g(t)$ are suitable estimates of Trotter error $|\Delta E_0|$. We performed calculations of these three error estimates on π -systems with up to 10 spatial orbitals. Our results are shown in Fig. 3.

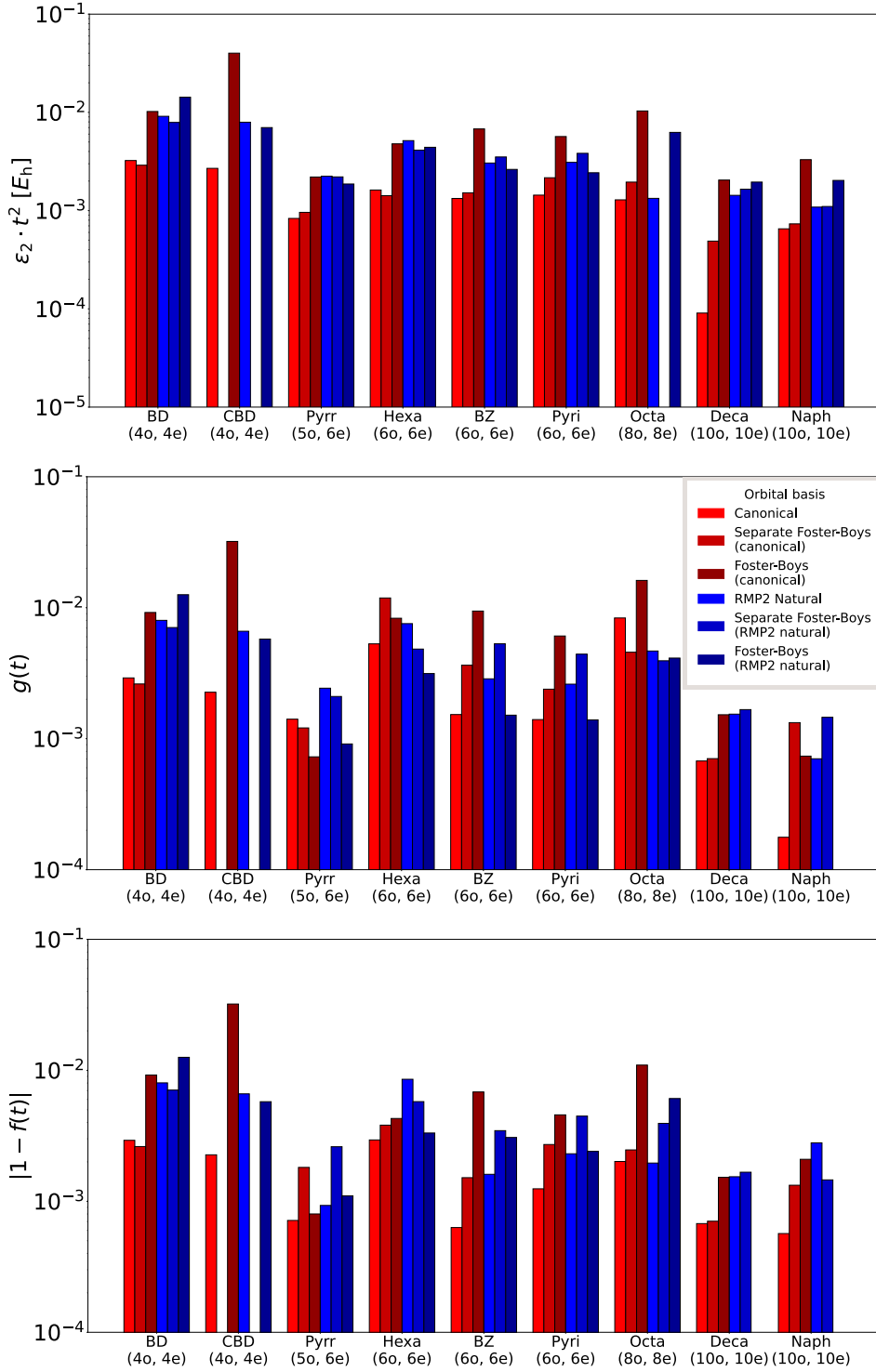


Figure 3: Estimates of Trotter error for the investigated π -systems. The fermionic Hamiltonian representation and magnitude ordering of the Trotter series were employed. Top: perturbation theory energy error estimate $\epsilon_2 t^2$. Middle: ACF offset $g(t)$. Bottom: infidelity $|1 - f(t)|$.

For the majority of cases, the employed energy error estimates agree on canonical orbital bases resulting in lower Trotter errors compared to localised bases. The estimate $\epsilon_2 t^2$ predicts that the Trotter error can vary by up to an order of magnitude between different orbital bases for π -systems with up to six spatial orbitals. This is consistent with results of Trotter error $|\Delta E_0|$ in Fig. 2. The estimate $\epsilon_2 t^2$ predicts that Trotter error incurred in different orbital bases can vary by up to more than one orders of magnitude if systems with

up to ten spatial orbitals are considered. We note, however, that the correlation between $|\Delta E_0|$ and $\epsilon_2 t^2$ was decreased for a qubit Hamiltonian representation.

4.2.2. Accounting for discrepancies in the ordering of terms in the Trotter series

We now assess the effect of differences in the Trotter series-ordering between the different orbital bases. While our previous choice of a magnitude ordering of the Trotter series was sensible, given that it typically incurs low Trotter errors [47], it resulted in a basis-dependent ordering of the terms \hat{H}_k , since the weights $|h_k|$ depend on the orbital basis. However, to isolate the effect of the orbital basis on Trotter error, a consistent Trotter series-ordering should be employed. We previously observed that a canonical orbital basis often incurred the lowest Trotter error. Hence, we performed calculations where the order of operators \hat{F}_k in the Trotter series matched that of the magnitude ordering of the canonical basis (see SI for additional information on this reordering); results are shown in Figs. 4 and 5.

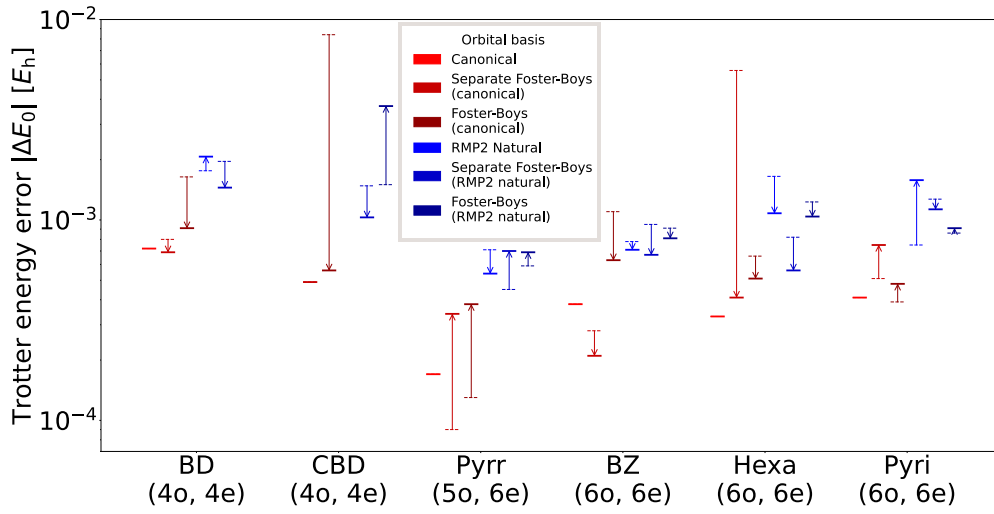


Figure 4: Trotter errors $|\Delta E_0|$ obtained to precision $\epsilon = 10^{-5} E_h$ (see Eqs. (45)-(47)) for active spaces of various π -systems in different orbital bases. Thin, dashed bars: a (basis-dependent) magnitude ordering of the Trotter series was employed (data previously shown in Fig. 2). Thick bars: the terms in the Trotter series were reordered to match the magnitude ordering of the canonical orbital basis.

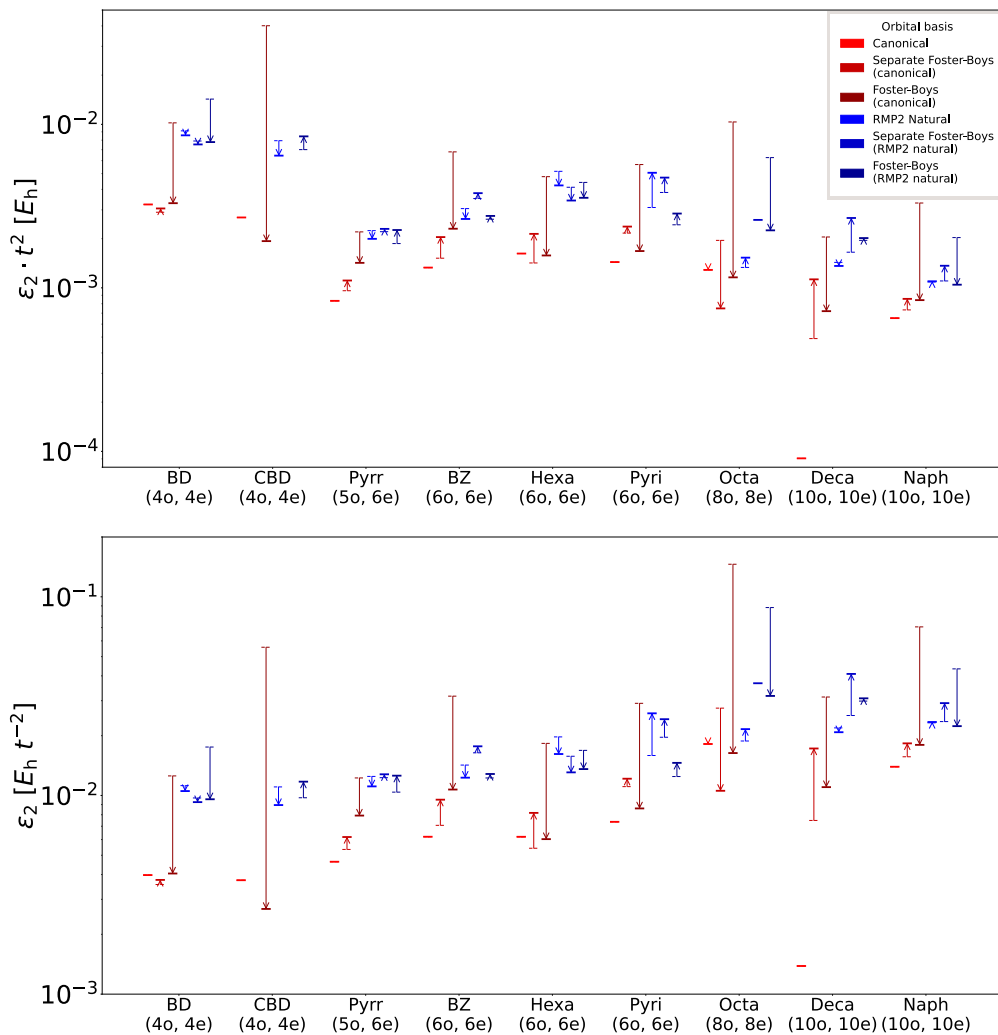


Figure 5: Trotter energy error estimates $\epsilon_2 t^2$ (top) and time-independent Trotter energy error estimates ϵ_2 (bottom) for active spaces of various π -systems in different orbital bases. Thin, dashed bars: a magnitude ordering of the Trotter series was employed (data previously shown in Fig. 3). Thick bars: the terms in the Trotter series were reordered to match the magnitude ordering of the canonical orbital basis.

The effect of changing the Trotter series-ordering to the magnitude ordering of the canonical basis, both on the Trotter error $|\Delta E_0|$ as well as the estimate ϵ_2 , can be notable. Up to an order of magnitude differences can be observed, and the largest differences are observed for a localised basis. For a fixed molecular system, both E_0 , and ϵ_2 now differ notably less between the different orbital bases upon consistent ordering of the operators \hat{F}_k . (Localised) canonical orbital bases now display consistently lower Trotter error compared to (localised) RMP2 natural orbital bases. The previous observation that a localised basis can substantially increase Trotter error can hence largely be attributed to differences in the Trotter series-ordering. Still, even with a basis-independent ordering of the Trotter series, an orbital basis which consistently incurs the lowest Trotter errors cannot be identified. However, the small variance of Trotter error in the different orbital bases suggests that the effect of the orbital basis on Trotter error can be much smaller compared to prior results [31]

We briefly comment on the growth of Trotter error with the number of active spatial orbitals N : Results for $|\Delta E_0|$ and $\epsilon_2 t^2$ in Figs. 4 and 5 suggest a decrease of Trotter error with system size. Note, however, that both of these quantities depend on the chosen Trotter

step number s . As listed in Table 1, we chose the time t per Trotter step to be proportional to the inverse of the ground state energy E_0 . It was also observed in Ref. [47] that choosing a Trotter step number s , such that $\frac{1}{s} \propto t \propto \frac{1}{E_0}$ can lead to Trotter errors (measured in Ref. [47] by a perturbative error estimate from Ref. [46]) that is decreasing with N . By contrast, a time-independent measure of Trotter error, such as ϵ_2 (see Fig. 5), shows that Trotter error (for fixed t) grows with N .

4.2.3. Correlation of descriptors with Trotter error

We summarise results on the correlation between estimates of Trotter error (or exact Trotter error) and easily obtainable descriptors of Trotter error in Table 2.

Trotter error (estimate)	1-norm λ_F	# of terms Γ
α^* , Eq. (29) [44]	0.836	0.652
$ \Delta E_0^* $ (23)	0.094	0.048
ϵ_2^* , Eq. (32) [27]	0.004	0.017
$\epsilon_2^* \cdot t^2$	0.187	0.136
ϵ_2^{all}	0.164	0.337
$\epsilon_2^{\text{all}} \cdot t^2$	0.139	0.092
$ \Delta E_0^{*,\text{cb}} $	0.071	0.091
$\epsilon_2^{*,\text{cb}}$	0.426	0.251
$\epsilon_2^{*,\text{cb}} \cdot t^2$	0.158	0.184
$\epsilon_2^{\text{all},\text{cb}}$	0.374	0.296
$\epsilon_2^{\text{all},\text{cb}} \cdot t^2$	0.296	0.249

Table 2: Pearson correlation coefficient R^2 of 1-norm λ_F and number of terms in the Hamiltonian Γ with various quantities describing the Trotter error in the energy: time-independent prefactor of the upper bound on Trotter error α , perturbation theory error estimate ϵ_2 and exact Trotter energy error $|\Delta E_0|$. The asterisk denotes that only π -systems with up to six spatial orbitals were considered. The superscript 'all' denotes that calculations on all π -systems (up to ten spatial orbitals) were considered. The superscript 'cb' indicates that the canonical basis magnitude ordering was employed instead of the basis-dependent magnitude ordering.

A notable correlation is observed between α , which is proportional to the upper bound on Trotter error, and both the 1-norm λ_F and the number of terms Γ in the Hamiltonian, as suggested by Eq. (29). However, no significant correlation of Trotter error $|\Delta E_0|$ or of the estimate ϵ_2 with λ_F is evident. Even a comparison of results with the canonical basis and separately localised basis, which preserves the single-reference character of $|\psi_0\rangle$, does not show a consistent reduction of Trotter error with the 1-norm. The results shown in Table 2 highlight that consistent ordering of the Trotter series in terms of the operators \hat{H}_k improved the correlation with the descriptors.

We conclude that the optimisation of circuit depth by a-priori selection of a low-Trotter-error orbital basis appears unfeasible. Descriptors such as the 1-norm and the number of non-negligible terms in the Hamiltonian depend solely on the orbital basis choice. They do not account for the notable dependence of Trotter error on the Trotter series-ordering. Consequently, it is challenging to find a descriptor which (i) can be easily evaluated, (ii) be optimised through orbital transformations, (iii) is correlated with Trotter error, and (iv) is independent of the Trotter series-ordering chosen.

4.3. Error cancellation with η -basis propagators and η -ordering propagators

Next, we investigate Trotter errors of η -basis propagators U_{rot} , and η -ordering propagators U_{reo} (see Eqs. (41) and (43)). η -basis propagators only feature benefits if they achieve either systematic error cancellation or an averaging effect of Trotter errors. Error cancellation means that the Trotter error $|\Delta E_0|$ associated with the propagator U_{rot} is smaller than the Trotter error of all of its constituent propagators $U_{\text{rot},n}$. Error averaging will be seen if the Trotter error associated with U_{rot} is below the average Trotter error of the constituent propagators $U_{\text{rot},n}$. Achieving systematic error averaging would already be useful, since it implies a lower Trotter error than that achieved in trotterised Hamiltonian simulation in a randomly selected fixed orbital basis.

In search of a simple error cancellation criterion, we studied Trotter errors of η -basis propagators and initially set $\eta = 2$ (i.e., only two orbital bases were employed in the construction of U_{rot}). As example systems, we considered (i) the HF molecule in a 6-31g basis set, with a (2o, 2e) orbital active space chosen around the Fermi level of the canonical orbital basis and (ii) molecular hydrogen in a minimal sto-3g basis set with a (2o, 2e) orbital active space, which corresponds to the Full CI active space. Since these active spaces contain only $N/2 = 2$ spatial orbitals, a single Givens rotation angle $\theta_{pq} \equiv \theta$ is sufficient to describe all possible orbital transformations as described by Eqs. (12) and (19).

For both examples, we constructed propagators U_{rot} according to Eq. (41) with $\eta = 2$, where $U_{\text{rot},1}$ is constructed in the orbital basis labeled θ_1 and $U_{\text{rot},2}$ is constructed in the orbital basis labeled θ_2 . We fixed the first orbital basis as $\theta_1 = 0$ and varied the second orbital basis θ_2 on the interval $\theta_2 \in [0, 2\pi)$. We compare the ground state energies of the effective Hamiltonians associated with the propagator U_{rot} and its constituents $U_{\text{rot},1}$ and $U_{\text{rot},2}$ in Fig. 6.

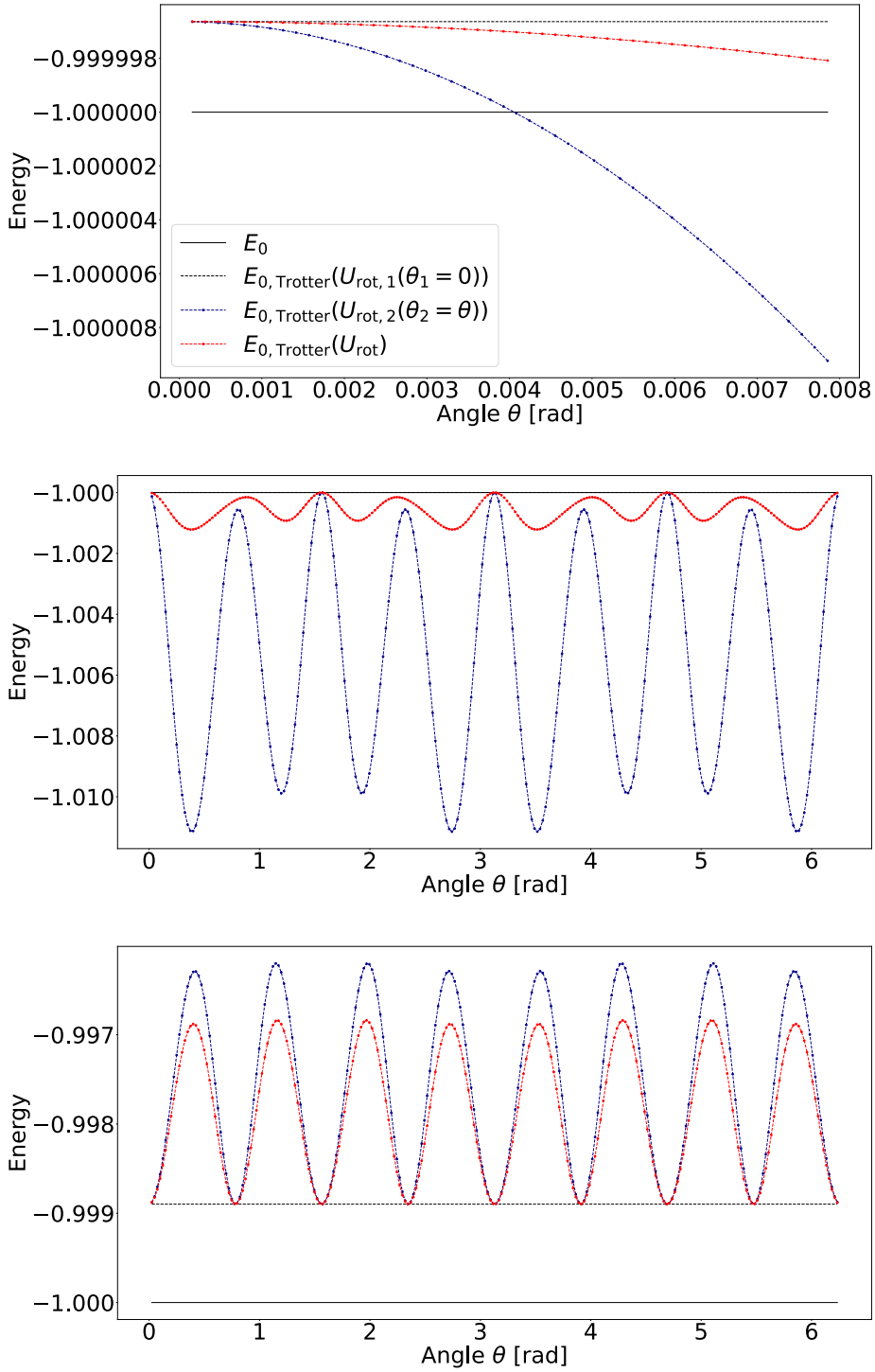


Figure 6: Ground state energies of the effective Hamiltonians of the η -basis propagator U_{rot} and its constituent propagators $U_{\text{rot},1}$ and $U_{\text{rot},2}$. The angle θ denotes the orbital basis employed in the construction of $U_{\text{rot},1}$ and $U_{\text{rot},2}$. The canonical orbital basis serves as the reference for $\theta = 0$. Normalised Hamiltonians were employed, such that the energy is unitless. The eigenvalue spectra of the Hamiltonians were shifted to the interval $[-1, 0]$, and the time evolution lengths was $t = 0.95\pi$. A fermionic Hamiltonian representation and the index-dependent Trotter series-ordering described in the SI were chosen. Top and middle: HF molecule at equilibrium bond length in a 6-31g basis with the active space chosen around the Fermi level. Top: small angle range for $\theta_2 = \theta$. Middle: period $\theta \in [0, 2\pi)$ in the angle. Bottom: hydrogen molecule at equilibrium bond length in a sto-3g basis for a full period in the angle θ .

As is apparent from Fig. 6, the ground state energy $E_{0,\text{Trotter}}$ associated with the propagator U_{rot} lies between that of its constituents $U_{\text{rot},1}$ and $U_{\text{rot},2}$. As such, error averaging is observed consistently. A straightforward condition required for error cancellation which goes beyond an averaging effect can be observed: the Trotter errors ΔE_0 of the bases θ_1 and θ_2 are of opposite sign.

For the HF molecule in the interval of $\theta_2 \in [0.006, 0.008]$, we can observe that this leads to error cancellation. For the hydrogen molecule, the error cancellation condition cannot be met, since Trotter error has a positive sign for every possible orbital basis.

If combining orbital bases with opposite-sign Trotter error is a required condition for error cancellation, then Fig. 6 suggests that error cancellation is unlikely to be achieved by Hamiltonian simulation with randomised orbital rotations between Trotter steps for the HF molecule. This is because Trotter errors are not symmetrically distributed around $\Delta E_0 = 0$ on the interval $\theta \in [0, 2\pi)$ which contains all orbital bases accessible by orbital transformations. Additionally, for both the hydrogen molecule and the HF molecule, the canonical orbital basis ($\theta = 0$) incurs a small Trotter error compared to a randomly selected basis θ . Hence, for both molecules, we expect Hamiltonian simulation in a fixed canonical basis to produce smaller Trotter errors $|\Delta E_0|$ compared to η -basis propagators, which are constructed from η randomly chosen orbital bases.

4.3.1. Distributions of Trotter error

Error cancellation might also be observed for the $\eta(= 2)$ -ordering propagator U_{reo} in Eq. (43), if its constituents $U_{\text{reo},1}$ and $U_{\text{reo},2}$ yield Trotter errors of opposite sign. However, for molecules with large active spaces N , we cannot determine the sign of the Trotter error of an orbital basis $\vec{\theta}_n$ (or a Trotter series-ordering $\vec{\sigma}_n$), since E_0 is unknown. We therefore require that a randomly selected set of orbital bases $\{\vec{\theta}_n\}_{n=1}^\eta$ (or orderings of the Trotter series $\{\vec{\sigma}_n\}_{n=1}^\eta$) contains a similar number of orbital bases (or orderings of the Trotter series) with positive and negative Trotter error. This necessitates that the distribution of Trotter error in the different orbital bases (or the different orderings of the Trotter series) itself is symmetrical around $\Delta E_0 = 0$. To assess whether error cancellation can be achieved with randomly constructed η -basis propagators U_{rot} and η -ordering propagators U_{reo} , we therefore investigated the distributions of Trotter error in the orbital basis θ and the ordering of the Trotter series $\vec{\sigma}$. Our results are shown in Fig. 7.

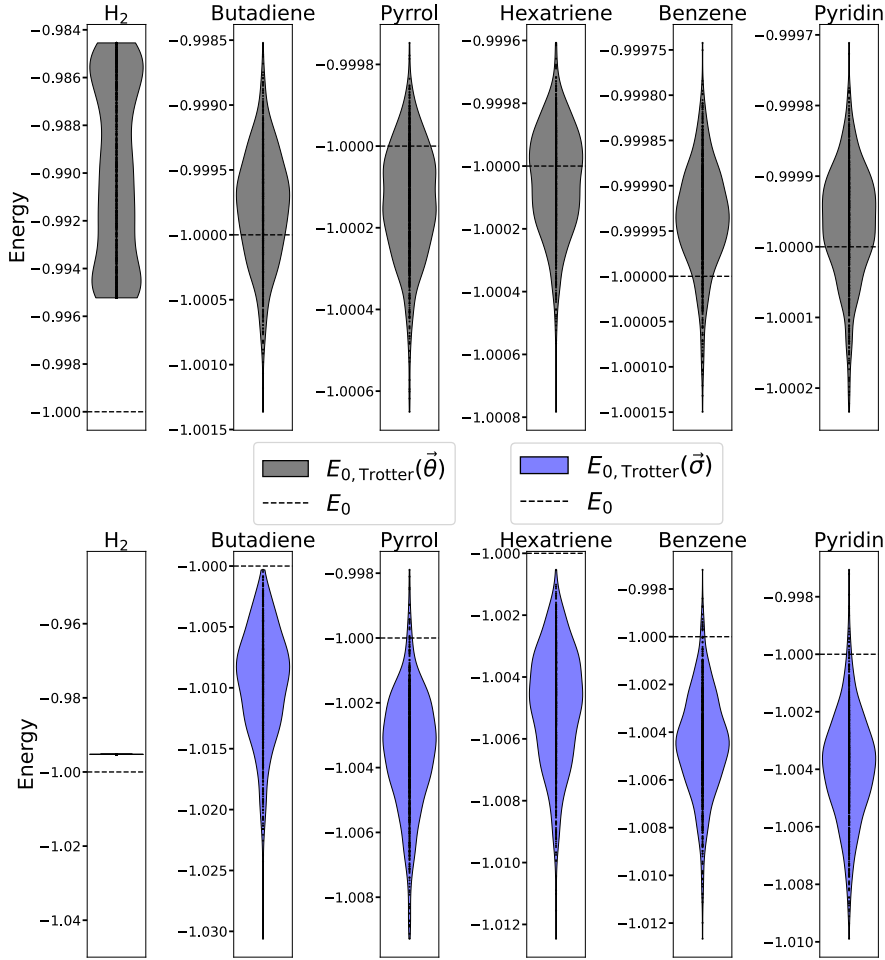


Figure 7: Distribution of the ground state energy $E_{0, \text{Trotter}}$ of the effective Hamiltonian of U_{Trotter} in Eq. (21) obtained from sampling 1000 randomly selected orbital bases $\vec{\theta}$ (top) and 1000 randomly selected orderings $\vec{\sigma}$ of the Trotter series (bottom) for various molecules. Normalised, fermionic Hamiltonians were employed so that the energy is unitless. A time step of $t = 0.95\pi$ was employed. Eigenvalue spectra were shifted to the interval $[-1, 0]$. The exact ground state energy (dashed, horizontal black line) is shown as a reference. Black dots indicate individual data points. We include the hydrogen molecule in a sto-3g basis and the π -systems (with details on the active spaces provided in Table 1). In the construction of η -basis propagators, the index-based Trotter series-ordering described in the SI was applied. For η -ordering propagators, we chose the Foster-Boys localised canonical orbital basis for all molecules, except for the hydrogen molecule, for which the canonical basis was picked instead.

As can be seen in Fig. 7, the Trotter error for the hydrogen molecule is unaffected by the ordering of the Trotter series. The distributions of $E_{0, \text{Trotter}}$ are not symmetric around E_0 . Hence, the distributions of Trotter error ΔE_0 are not symmetric around zero. Among the examined distributions, the distribution of Trotter error in the orbital basis with a fermionic Hamiltonian representation is most symmetrical. Surprisingly, negatively signed Trotter errors rarely occurred, independent of basis choice and ordering of the Trotter series with a qubit Hamiltonian representation (see the SI). As a result, we can generally not expect trotterised propagators with random basis transformations to reduce the Trotter error.

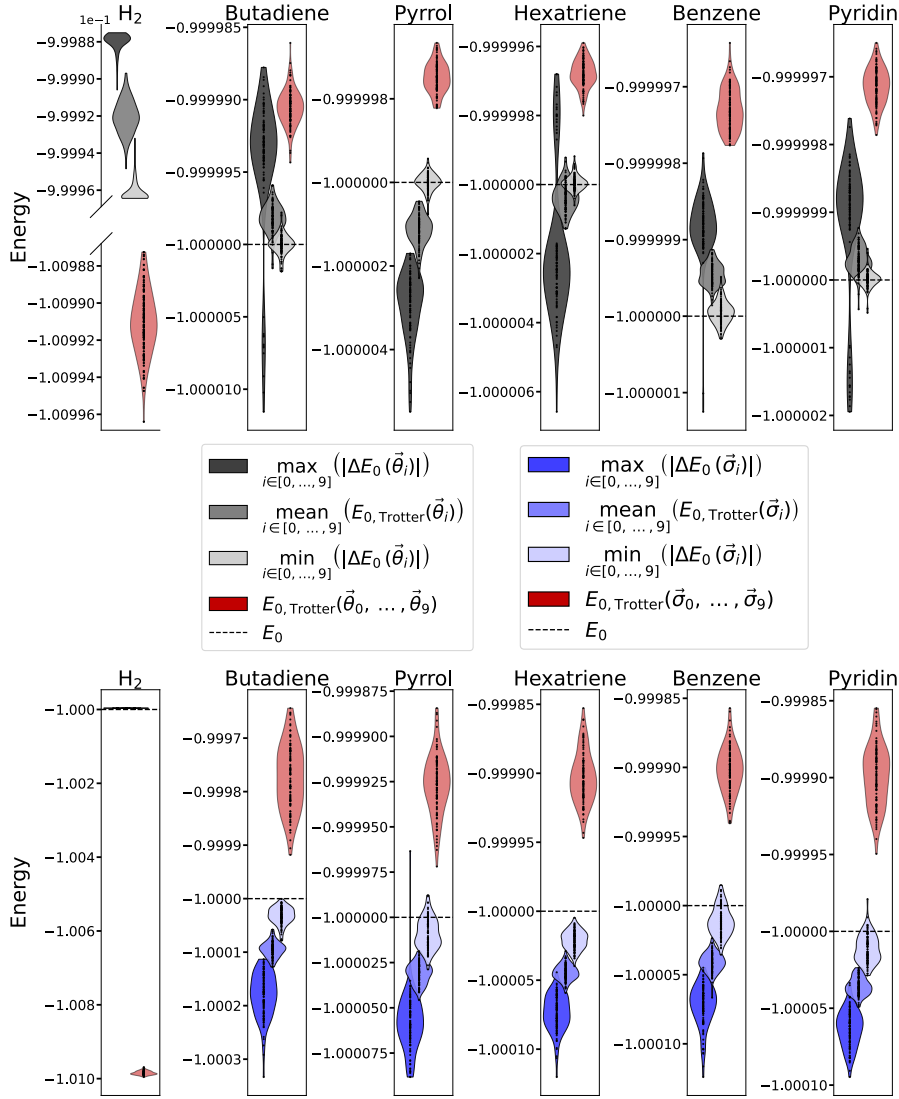


Figure 8: Top: Distributions of the ground state energy of the effective Hamiltonians of 100 randomly constructed propagators U_{rot} (red). Distributions of the ground state energy of the effective Hamiltonians of the constituent propagators $U_{\text{rot},n}$ that are associated with the largest (dark grey), average (grey), and smallest absolute value (light grey) Trotter error. Bottom: Analogous comparison between randomised series ordering propagators U_{reo} (red) and their constituents $U_{\text{reo},n}$ exhibiting largest (dark blue), average (blue), and smallest absolute value (light blue) Trotter error. For the construction of η -basis propagators U_{rot} , the index-dependent Trotter series-orderings described in the SI was applied. For the construction of U_{reo} , the chosen fixed basis $\vec{\theta}$ was the Foster-Boys localised canonical orbital basis for all molecules, except for molecular hydrogen, for which the canonical orbital basis was picked instead. Normalised Hamiltonians were employed so that the energy is unitless. An evolution time span of $t = 0.95\pi$ was set. Eigenvalue spectra were shifted to the interval $[-1,0]$. Black dots indicate individual data points. Data are shown for a fermionic Hamiltonian representation.

4.3.2. Trotter error of η -basis propagators and η -ordering-propagators with $\eta > 2$

Finally, we investigate the Trotter error of η -basis propagators constructed from randomly selected orbital basis (and η -ordering propagators constructed from randomly selected

Trotter series-orderings) with $\eta > 2$. For the molecules in Fig. 7, we constructed 100 distinct propagators U_{rot} (with $\eta = 10$) from the constituent propagators $U_{\text{rot},n}$. The orbital basis $\vec{\theta}_n$ of each constituent propagator $U_{\text{rot},n}$ was randomly selected. Fig. 8 shows the distribution of the ground state energies $E_{0,\text{Trotter}}$ of the effective Hamiltonians of 100 η -basis propagators U_{rot} . η -ordering propagators U_{reo} were constructed and assessed in an analogous fashion.

A shift towards positive-sign Trotter errors for the η -basis propagators and η -ordering propagators is observed for all systems (except for the dihydrogen). This observation holds true for both the fermionic (Fig. 8), and for the qubit Hamiltonian representations (see the SI). Additionally, the previous observation, namely that error cancellation or averaging can be achieved by combination of trotterised propagators, which incur oppositely signed Trotter error, is inapplicable to η -basis propagators and η -ordering propagators with η larger than two. This is apparent for the η -ordering propagators of butadiene and hexatriene shown in Fig. 8: not a single propagator $U_{\text{reo},n}$ in U_{reo} incurred a positively signed Trotter error. A positively signed Trotter error is, however, consistently observed for the propagators U_{reo} . For the fermionic Hamiltonian representation, we observe that η -basis propagators U_{rot} incur a Trotter error $|\Delta E_0|$, which is comparable to the largest Trotter error achieved by one of the ten propagators $U_{\text{rot},n}$ from which U_{rot} is constructed. A similar observation can be made for η -ordering propagators U_{reo} . Consequently, neither error averaging, nor error cancellation was observed for η -basis propagators or η -ordering propagators. For the qubit Hamiltonian representation, we consistently observe U_{rot} and U_{reo} to produce larger Trotter error compared to all propagators $U_{\text{rot},n}$ and $U_{\text{reo},n}$ used for their construction. Consequently, our results suggest that η -basis propagators and η -ordering propagators lead to error magnification, rather than error cancellation or averaging of the Trotter error.

5. Conclusions

We have assessed three strategies to reduce ground-state-energy Trotter error by orbital basis transformations.

(i) We investigated whether the selection of a low Trotter error orbital basis can be made before carrying out an actual quantum computation in order to reduce the resource cost of QPE. To this end, we studied whether simple descriptors, which depend solely on the employed orbital basis and which can be optimised through orbital transformations, correlate with Trotter error. Despite analytical expressions suggesting that these descriptors should correlate with Trotter error, poor correlation was observed in practice. This poor correlation we attribute in parts to their inability to account for the effect of Trotter series ordering, known to significantly affect Trotter error [47]. We found a reduced spread of ground-state Trotter error for standard orbital bases of π -systems compared to the atomic systems investigated in Ref. [31]. This suggests that the choice of a low Trotter error orbital basis is of limited importance in practice. Consequently, the reduction of the gate count per Trotter step emerges as a more suitable avenue to reduce Hamiltonian simulation cost for QPE. It is already well-established that localised orbital bases can reduce the gate count per Trotter step, since they maximise the number of terms in the Hamiltonian that can be neglected due to small coefficient weights [56, 57].

(ii) We observed that the Trotter error of the ground state energy is a continuous function of the transformed orbital basis if an index-based Trotter series ordering is applied. We proposed that this continuity might be exploitable and allow for the determination of an orbital basis in which the ground state energy is free of Trotter error. QPE with trotterised Hamiltonian simulation would allow exact calculations of the ground state energy in such an Trotter-error-free orbital basis. However, if only an upper and lower bound on E_0 are

known, the determination of this error-free basis can be challenging.

(iii) We investigated whether changing the orbital basis between Trotter steps can reduce the Trotter error. If we alternate the orbital bases between Trotter steps where a negatively signed Trotter error ($\Delta E_0 < 0$) is combined with a positively signed Trotter error ($\Delta E_0 > 0$), error averaging naturally occurs, and in some cases this leads to error cancellation. However, for large active spaces, we cannot determine whether an orbital basis has a positively or negatively signed Trotter error prior to a quantum computation. Additionally, results for trotterised propagators, which employ up to ten different orbital bases in their construction, suggest error magnification rather than error cancellation or averaging for propagators with a dynamical basis. Hence, propagators which randomise the orbital basis are unlikely to reduce Trotter error in practice.

If the derivation of tighter bounds on Trotter error by randomisation of the orbital basis would be possible, trotterised Hamiltonian simulation with a dynamical orbital basis could, however, still be useful if a simulation with accuracy-guaranteed precision is desired. A remaining possibility to explore orbital transformations in the context of Hamiltonian simulation with product formulae is the inclusion of orbital transformations in the qDRIFT protocol. Whether this allows for the derivation of tighter Trotter error bounds compared to a fixed orbital basis qDRIFT protocol needs to be studied in future work.

We conclude that, while orbital transformations can be straightforwardly leveraged to reduce the gate depth of a single Trotter step, consistent reductions in Trotter error are very difficult to achieve by orbital transformation. Importantly, we could not find evidence that localised orbitals incur notably higher Trotter error compared to other choices of orbital basis sets. Consequently, our results reconfirm the use of localised orbital basis for shallower QPE circuits.

Acknowledgements

We gratefully acknowledge generous financial support by the Swiss National Science Foundation (grant no. 200021_219616) and by the Novo Nordisk Foundation (grant no. NNF20OC0059939 ‘Quantum for Life’).

Author contributions

All authors contributed equally to the conceptualisation of this work. M.K. and M.E. wrote the software and M.K. carried out the calculations. All authors analysed the results and prepared the manuscript. M.R. acquired funding, computing resources, and supervised the project. M.R. is the corresponding author.

Disclosure statement

The authors declare no conflict of interest.

Data availability statement

The data that support the findings of this study will be made available as a zenodo repository.

References

- [1] A. Baiardi and M. Reiher, *J. Chem. Phys.* **152**, 040903 (2020).
- [2] F.A. Evangelista, *J. Chem. Phys.* **149**, 030901 (2018).

- [3] A.Y. Sokolov, *Adv. Quantum Chem.* **90**, 121–155 (2024).
- [4] J.W. Park, R. Al-Saadon, M.K. MacLeod, T. Shiozaki and B. Vlaisavljevich, *Chem. Rev.* **120**, 5878–5909 (2020).
- [5] M.A. Nielsen and I.L. Chuang, *Quantum computation and quantum information* (Cambridge university press, Cambridge, 2010).
- [6] A.Y. Kitaev, preprint, arXiv:quant-ph/9511026 (1995).
<<http://arxiv.org/abs/quant-ph/9511026>>.
- [7] D.S. Abrams and S. Lloyd, *Phys. Rev. Lett.* **83**, 5162 (1999).
- [8] A. Aspuru-Guzik, A.D. Dutoi, P.J. Love and M. Head-Gordon, *Science* **309**, 1704–1707 (2005).
- [9] J.D. Whitfield, J. Biamonte and A. Aspuru-Guzik, *Mol. Phys.* **109**, 735–750 (2011).
- [10] T. Helgaker, P. Jorgensen and J. Olsen, *Molecular electronic-structure theory* (John Wiley & Sons, New Jersey, 2013).
- [11] M. Reiher, N. Wiebe, K.M. Svore, D. Wecker and M. Troyer, *Proc. Natl. Acad. Sci.* **114**, 7555–7560 (2017).
- [12] L.A. Martínez-Martínez, T.-C. Yen and A.F. Izmaylov, *Quantum* **7**, 1086 (2023).
- [13] D.W. Berry, C. Gidney, M. Motta, J.R. McClean and R. Babbush, *Quantum* **3**, 208 (2019).
- [14] V. von Burg, G.H. Low, T. Häner, D.S. Steiger, M. Reiher, M. Roetteler and M. Troyer, *Phys. Rev. Res.* **3**, 033055 (2021).
- [15] J. Lee, D.W. Berry, C. Gidney, W.J. Huggins, J.R. McClean, N. Wiebe and R. Babbush, *PRX Quantum* **2**, 030305 (2021).
- [16] M. Motta, E. Ye, J.R. McClean, Z. Li, A.J. Minnich, R. Babbush and G.K.-L. Chan, *npj Quantum Inf.* **7**, 83 (2021).
- [17] B. Peng and K. Kowalski, *J. Chem. Theory Comput.* **13**, 4179–4192 (2017).
- [18] Y. Su, D.W. Berry, N. Wiebe, N. Rubin and R. Babbush, *PRX Quantum* **2**, 040332 (2021).
- [19] T.N. Georges, M. Bothe, C. Sünderhauf, B.K. Berntson, R. Izsák and A.V. Ivanov, *npj Quantum Inf.* **11**, 55 (2025).
- [20] D. Rocca, C.L. Cortes, J.F. Gonthier, P.J. Ollitrault, R.M. Parrish, G.-L. Anselmetti, M. Degroote, N. Moll, R. Santagati and M. Streif, *J. Chem. Theory Comput.* **20**, 4639–4653 (2024).
- [21] G.H. Low, R. King, D.W. Berry, Q. Han, A.E. DePrince III, A.F. White, R. Babbush, R.D. Somma and N.C. Rubin, *Phys. Rev. X* **15**, 041016 (2025).
- [22] M. Erakovic, F. Witteveen, D. Harley, J. Günther, M. Bensberg, O.R. Meitei, M. Cho, T. Van Voorhis, M. Reiher and M. Christandl, *PRX Life* **3**, 013003 (2025).
- [23] M. Mörchen, G.H. Low, T. Weymuth, H. Liu, M. Troyer and M. Reiher, preprint, arXiv:2409.08910 (2024).
<<https://arxiv.org/abs/2409.08910>>.
- [24] N.M. Tubman, C. Mejuto-Zaera, J.M. Epstein, D. Hait, D.S. Levine, W. Huggins, Z. Jiang, J.R. McClean, R. Babbush, M. Head-Gordon et al., preprint, arXiv:1809.05523 (2018).
<<https://arxiv.org/abs/1809.05523>>.

- [25] D.W. Berry, M. Kieferová, A. Scherer, Y.R. Sanders, G.H. Low, N. Wiebe, C. Gidney and R. Babbush, *npj Quantum Inf.* **4**, 22 (2018).
- [26] W.J. Huggins, O. Leimkuhler, T.F. Stetina and K.B. Whaley, *PRX Quantum* **6**, 020319 (2025).
- [27] S.G. Mehendale, L.A. Martínez-Martínez, P.D. Kamath and A.F. Izmaylov, *Digit. Discov.* **4**, 3540–3551 (2025).
- [28] H.F. Trotter, *Proc. Am. Math. Soc.* **10**, 545–551 (1959).
- [29] M. Suzuki, *Commun. Math. Phys.* **51**, 183–190 (1976).
- [30] J.T. Seeley, M.J. Richard and P.J. Love, *J. Chem. Phys.* **137**, 224109 (2012).
- [31] R. Babbush, J. McClean, D. Wecker, A. Aspuru-Guzik and N. Wiebe, *Phys. Rev. A* **91**, 022311 (2015).
- [32] A.M. Childs and N. Wiebe, *Quantum Information and Computation* **12**, 901–924 (2012).
- [33] S. Zhuk, N.F. Robertson and S. Bravyi, *Phys. Rev. Res.* **6**, 033309 (2024).
- [34] G.H. Low and I.L. Chuang, *Quantum* **3**, 163 (2019).
- [35] R. Babbush, C. Gidney, D.W. Berry, N. Wiebe, J. McClean, A. Paler, A. Fowler and H. Neven, *Phys. Rev. X* **8**, 041015 (2018).
- [36] D. Poulin, A. Kitaev, D.S. Steiger, M.B. Hastings and M. Troyer, *Phys. Rev. Lett.* **121**, 010501 (2018).
- [37] J. Günther, F. Witteveen, A. Schmidhuber, M. Miller, M. Christandl and A. Harrow, preprint, arXiv:2503.05647 (2025).
<<https://arxiv.org/abs/2503.05647>>.
- [38] Z. Li, J. Li, N.S. Dattani, C. Umrigar and G.K. Chan, *J. Chem. Phys.* **150**, 024302 (2019).
- [39] J.J. Goings, A. White, J. Lee, C.S. Tautermann, M. Degroote, C. Gidney, T. Shiozaki, R. Babbush and N.C. Rubin, *Proc. Natl. Acad. Sci.* **119**, e2203533119 (2022).
- [40] S. Hariharan, S. Kinge and L. Visscher, *J. Chem. Inf. Model.* **65**, 472–511 (2024).
- [41] S.N. Genin, I.G. Ryabinkin, N.R. Paisley, S.O. Whelan, M.G. Helander and Z.M. Hudson, *Angew. Chem. Int. Ed.* **61**, e202116175 (2022).
- [42] S. Lee, J. Lee, H. Zhai, Y. Tong, A.M. Dalzell, A. Kumar, P. Helms, J. Gray, Z.-H. Cui, W. Liu et al., *Nature communications* **14**, 1952 (2023).
- [43] N. Maskara, S. Ostermann, J. Shee, M. Kalinowski, A. McClain Gomez, R. Araiza Bravo, D.S. Wang, A.I. Krylov, N.Y. Yao, M. Head-Gordon et al., *Nat. Phys.* **21**, 289–297 (2025).
- [44] A.M. Childs, Y. Su, M.C. Tran, N. Wiebe and S. Zhu, *Phys. Rev. X* **11**, 011020 (2021).
- [45] A.M. Childs and Y. Su, *Phys. Rev. Lett.* **123**, 050503 (2019).
- [46] D. Poulin, M. Hastings, D. Wecker, N. Wiebe, A.C. Doberty and M. Troyer, *Quant. Inf. Comput.* **15**, 0361–0384 (2015).
- [47] A. Tranter, P.J. Love, F. Mintert, N. Wiebe and P.V. Coveney, *Entropy* **21**, 1218 (2019).
- [48] M. Luo and J.I. Cirac, *PRX Quantum* **6**, 010355 (2025).

- [49] E.G. Hohenstein, R.M. Parrish and T.J. Martínez, *J. Chem. Phys.* **137**, 044103 (2012).
- [50] R.M. Parrish, E.G. Hohenstein, T.J. Martínez and C.D. Sherrill, *J. Chem. Phys.* **137**, 224106 (2012).
- [51] E.G. Hohenstein, R.M. Parrish, C.D. Sherrill and T.J. Martínez, *J. Chem. Phys.* **137**, 221101 (2012).
- [52] S. Jin and X. Li, *Commun. Appl. Math. Comput.* **7**, 442–469 (2025).
- [53] M. Hagan and N. Wiebe, *Quantum* **7**, 1181 (2023).
- [54] A.M. Childs, A. Ostrander and Y. Su, *Quantum* **3**, 182 (2019).
- [55] E. Campbell, *Phys. Rev. Lett.* **123**, 070503 (2019).
- [56] E. Koridon, S. Yalouz, B. Senjean, F. Buda, T.E. O’Brien and L. Visscher, *Phys. Rev. Res.* **3**, 033127 (2021).
- [57] J.R. McClean, R. Babbush, P.J. Love and A. Aspuru-Guzik, *J. Phys. Chem. Lett.* **5**, 4368–4380 (2014).
- [58] M.B. Hastings, D. Wecker, B. Bauer and M. Troyer, *Quantum Information & Computation* **15**, 1–21 (2015).
- [59] P. Mukhopadhyay, N. Wiebe and H.T. Zhang, *npj Quantum Inf.* **9**, 31 (2023).
- [60] I.D. Kivlichan, J. McClean, N. Wiebe, C. Gidney, A. Aspuru-Guzik, G.K.-L. Chan and R. Babbush, *Phys. Rev. Lett.* **120**, 110501 (2018).
- [61] M. Motta, E. Ye, J.R. McClean, Z. Li, A.J. Minnich, R. Babbush and G.K.-L. Chan, *npj Quantum Inf.* **7**, 83 (2021).
- [62] N.C. Rubin, J. Lee and R. Babbush, *J. Chem. Theory Comput.* **18**, 1480–1488 (2022).
- [63] J.M. Arrazola, O. Di Matteo, N. Quesada, S. Jahangiri, A. Delgado and N. Killoran, *Quantum* **6**, 742 (2022).
- [64] F.L. Buessen, D. Segal and I. Khait, *Phys. Rev. Res.* **5**, L022003 (2023).
- [65] D. Burgarth, P. Facchi, A. Hahn, M. Johansson and K. Yuasa, *Phys. Rev. Res.* **6**, 043155 (2024).
- [66] C. Yi and E. Crosson, *npj Quantum Inf.* **8**, 37 (2022).
- [67] M. Miller, J. Günther, F. Witteveen, M.S. Teynor, M. Erakovic, M. Reiher, G.C. Solomon and M. Christandl, preprint, arXiv:2504.17881 (2025).
<<https://arxiv.org/abs/2504.17881>>.
- [68] L.A. Martínez-Martínez, P.D. Kamath and A.F. Izmaylov, preprint, arXiv:2312.13282v2 (2023).
<<https://arxiv.org/abs/2312.13282v2>>.
- [69] C. Zhang, *Monte Carlo and Quasi-Monte Carlo Methods 2010* (Springer, Heidelberg, 2012), pp. 709–719.
- [70] R. Trivedi and J.I. Cirac, preprint, arXiv:2509.17579 (2025).
<<https://arxiv.org/abs/2509.17579>>.
- [71] N. Goldman and J. Dalibard, *Phys. Rev. X* **4**, 031027 (2014).
- [72] S. Kim, J. Chen, T. Cheng, A. Gindulyte, J. He, S. He, Q. Li, B.A. Shoemaker, P.A. Thiessen, B. Yu et al., *Nucleic Acids Res.* **47**, D1102–D1109 (2019).

- [73] L.-P. Wang and C. Song, *J. Chem. Phys.* **144**, 214108 (2016).
- [74] A.D. Becke, *J. Chem. Phys.* **98**, 5648–5652 (1993).
- [75] T.H. Dunning Jr, *J. Chem. Phys.* **90**, 1007–1023 (1989).
- [76] W.J. Hehre, R.F. Stewart and J.A. Pople, *J. Chem. Phys.* **51**, 2657–2664 (1969).
- [77] J. Foster and S. Boys, *Rev. Mod. Phys.* **32**, 300 (1960).
- [78] Q. Sun, T.C. Berkelbach, N.S. Blunt, G.H. Booth, S. Guo, Z. Li, J. Liu, J.D. McClain, E.R. Sayfutyarova, S. Sharma et al., *Wiley Interdiscip. Rev. Comput. Mol. Sci.* **8**, e1340 (2018).
- [79] V. Bergholm, J. Izaac, M. Schuld, C. Gogolin, S. Ahmed, V. Ajith, M.S. Alam, G. Alonso-Linaje, B. AkashNarayanan, A. Asadi et al., preprint, arXiv:1811.04968 (2018).
<<https://arxiv.org/abs/1811.04968>>.
- [80] P. Jordan and E.P. Wigner, *Zs. f. Phys.* **47**, 631–651 (1928).
- [81] K. Szenes, N. Glaser, M. Erakovic, V. Barandun, M. Morchen, R. Feldmann, S. Battaglia, A. Baiardi and M. Reiher, *J. Phys. Chem. A* **129**, 7549–7574 (2025).
- [82] K. Boguslawski, K.H. Marti and M. Reiher, *J. Chem. Phys.* **134**, 224101 (2011).
- [83] J.R. McClean, N.C. Rubin, K.J. Sung, I.D. Kivlichan, X. Bonet-Monroig, Y. Cao, C. Dai, E.S. Fried, C. Gidney, B. Gimby et al., *Quantum Sci. Technol.* **5**, 034014 (2020).
- [84] P. Virtanen, R. Gommers, T.E. Oliphant, M. Haberland, T. Reddy, D. Cournapeau, E. Burovski, P. Peterson, W. Weckesser, J. Bright et al., *Nat. Methods* **17**, 261–272 (2020).
- [85] L.A. Martínez-Martínez et al., *TrueTrotterError* (2022).
<https://github.com/pratham11/TrueTrotterError/tree/main> (accessed May 5, 2025).
- [86] C.E. Shannon, *Proc. IRE* **37**, 10–21 (1949).
- [87] A. Baiardi and M. Reiher, *J. Chem. Theory Comput.* **15**, 3481–3498 (2019).
- [88] J.D. Hunter, *Comput. Sci. Eng.* **9**, 90–95 (2007).
- [89] Y. Kurashige and T. Yanai, *Bull. Chem. Soc. Jpn.* **87**, 1071–1073 (2014).
- [90] H.F. Bettinger, C. Tönshoff, M. Doerr and E. Sanchez-Garcia, *J. Chem. Theory Comput.* **12**, 305–312 (2016).